© 2014. Published by The Company of Biologists Ltd | Journal of Cell Science (2014) 127, 3687–3698 doi:10.1242/jcs.146662

RESEARCH ARTICLE

Intracellular glycine receptor function facilitates glioma formation *in vivo*

Benjamin Förstera[1,*], Omar Dildar a Dzaye[2,*], Aline Winkelmann[1,3], Marcus Semtner[1], Bruno Benedetti[4], Darko S. Markovic[5], Michael Synowitz[6], Peter Wend[7], Michael Fähling[8], Marie-Pierre Junier[9], Rainer Glass[10], Helmut Kettenmann[2] and Jochen C. Meier[1,‡]

ABSTRACT

The neuronal function of Cys-loop neurotransmitter receptors is established; however, their role in non-neuronal cells is poorly defined. As brain tumors are enriched in the neurotransmitter glycine, we studied the expression and function of glycine receptors (GlyRs) in glioma cells. Human brain tumor biopsies selectively expressed the GlyR α1 and α3 subunits, which have nuclear localization signals (NLSs). The mouse glioma cell line GL261 expressed GlyR α1, and knockdown of GlyR α1 protein expression impaired the self-renewal capacity and tumorigenicity of GL261 glioma cells, as shown by a neurosphere assay and GL261 cell inoculation *in vivo*, respectively. We furthermore showed that the pronounced tumorigenic effect of GlyR α1 relies on a new intracellular signaling function that depends on the NLS region in the large cytosolic loop and impacts on GL261 glioma cell gene regulation. Stable expression of GlyR α1 and α3 loops rescued the self-renewal capacity of GlyR α1 knockdown cells, which demonstrates their functional equivalence. The new intracellular signaling function identified here goes beyond the well-established role of GlyRs as neuronal ligand-gated ion channels and defines NLS-containing GlyRs as new potential targets for brain tumor therapies.

KEY WORDS: Glycine receptor, Gene regulation, Glioma

INTRODUCTION

Glycine receptors (GlyRs) belong to the Cys-loop neurotransmitter receptor family of ligand-gated ion channels. Members of this receptor family have a similar protein architecture, with an extracellular ligand-binding domain, four transmembrane segments and a large cytosolic loop domain between transmembrane segments 3 and 4. Four genes (*Glra1–Glra4*) coding for GlyR α1–α4 subunits have been identified, and each of these subunits is able to produce functional homomeric glycine-gated Cl^- channels (Harvey et al., 2000; Kuhse et al., 1991; Malosio et al., 1991; Nikolic et al., 1998). In humans, however, *GLRA4* is a pseudogene (Simon et al., 2004). A single gene (*Glrb*) delivers cells with the GlyR β subunit, which mediates postsynaptic receptor anchoring (Meier et al., 2001; Meyer et al., 1995) and can contribute to glycine binding (Grudzinska et al., 2005), but is unable to produce functional homo-pentameric GlyR channels. GlyR α1 and α3 structurally differ from the α2, α4 or β subunits as they contain a functional nuclear localization signal (NLS) in the large cytosolic loop domain (Melzer et al., 2010). It has been established that the NLS interacts with nuclear import proteins of the karyopherin family (importin α3 and α4) (Melzer et al., 2010), but although the functional role of this sequence determinant has remained elusive, it has been suggested to play a role in non-neuronal cells (den Eynden et al., 2009). Brain tumors are enriched in the neurotransmitter glycine (Bobek-Billewicz et al., 2010), which raises the question as to whether glioma cell GlyRs serve a classical neurotransmitter receptor function or use their NLS for intracellular signaling.

Here, we addressed this question and discovered that the NLS-harboring GlyR α1 and α3 subunits were expressed in human brain tumor biopsies. We found that glioma cell GlyRs were retained in intracellular compartments and did not serve as neurotransmitter receptors. To study the functional role of intracellular GlyR expression in glioma cells, we used the mouse glioma cell line GL261, which specifically expresses the GlyR α1ins RNA splice variant (Malosio et al., 1991) with hitherto unknown function. Knockdown of GlyR α1ins protein expression impaired tumorigenicity and self-renewal capacity. The pronounced anti-tumor effect of reduced GlyR α1ins protein expression relied on an intracellular GlyR signaling function that was mediated by the large cytosolic loop domain, including the GlyR-intrinsic NLS, which ultimately regulated the expression of tumor cell genes. The GlyR target genes included proto-oncogenes, molecules involved in signaling pathways downstream of extracellular-signal-regulated kinase (ERK) and β-catenin/Wnt, transcription factors, and a plethora of gene products that are known to be involved in determining self-renewal capacity (‘stemness’). That the self-renewal capacity of GlyR α1ins knockdown GL261 cells was rescued upon stable expression of the GlyR α1ins and α3K loops furthermore demonstrates the functional equivalence of both GlyR subunits in brain tumor cells.

[1]RNA editing and Hyperexcitability Disorders Helmholtz Group, Max Delbrück Center for Molecular Medicine, 13092 Berlin, Germany. [2]Cellular Neuroscience, Max Delbrück Center for Molecular Medicine, 13092 Berlin, Germany. [3]FU-Berlin, Fachbereich Biologie, Chemie, Pharmazie, Takustrasse 3, 14195 Berlin. [4]Department for Physiology, Innsbruck Medical University, 6020 Innsbruck, Austria. [5]Department for Neurosurgery, Helios Clinic Buch, 13125 Berlin, Germany. [6]Department for Neurosurgery, Charité Universitätsmedizin Berlin, 13353 Berlin, Germany. [7]David Geffen School of Medicine at UCLA, UCLA Jonsson Comprehensive Cancer Center, 10833 LeConte Avenue, CHS 27-139, Los Angeles, CA. 90095, USA. [8]Institut für Vegetative Physiologie, Charité Universitätsmedizin Berlin, 10117 Berlin, Germany. [9]INSERM U894, Psychiatry and Neuroscience Center, Glial Plasticity Team, Paris 75014, France. [10]Neurosurgical Research, University Clinics Munich, 81377 München, Germany.
*These authors contributed equally to this work

‡Author for correspondence (jochen.meier@mdc-berlin.de)

Received 20 November 2013; Accepted 16 June 2014

Journal of Cell Science (2014) 127, 3687–3698 doi:10.1242/jcs.146662

RESULTS

GlyR α1 and α3 are expressed in human brain tumors and stem cells

To study GlyR expression in human glioma biopsies, quantitative real-time PCR analysis of GlyR α1-, α2- and α3-encoding mRNA was performed on a β-actin-normalized cDNA panel of pathologist-verified human brain tumors (supplementary material Table S1). We did not include the α4 subunit into our analyses because this type of GlyR will not form functional glycine-gated receptor channels at the cell surface due to a premature stop codon encoded in the human *GLRA4* gene (Simon et al., 2004). Following amplification of the samples, PCR products were analyzed with agarose gel electrophoresis, and a sample was only included into our quantitative expression analysis if a single band with the correct molecular mass was detected. *GLRA1* gene expression was detected primarily in World Health Organization (WHO) grade II and III tumors, whereas *GLRA3* gene expression was more widespread and found throughout WHO grade I–IV tumors (Fig. 1; supplementary material Table S1). GlyR α2-encoding mRNA was not detected (except case number 36).

We next analyzed expression of GlyR α1 and α3 subunits in established and well-characterized human stem-cell-like glioma cells (Galan-Moya et al., 2011; Silvestre et al., 2011; Thirant et al., 2011) (supplementary material Table S2). mRNA coding for the GlyR α1ins RNA splice variant (Malosio et al., 1991) was detected in three out of six stem-cell-like cell samples from adult oligoastrocytoma and glioblastoma multiforme (Galan-Moya et al., 2011; Silvestre et al., 2011), whereas GlyR α1-encoding mRNA in stem-cell-like cells from pediatric glioma (Thirant et al., 2011) lacked the RNA splice insert (supplementary material Table S2). GlyR α3-coding mRNA was detected in all the analyzed samples (supplementary material Table S2). Moreover, the vast majority (nine out of 11) of stem-cell-like cells expressed the GlyR α3K RNA splice variant (Nikolic et al., 1998), which sets this cell type apart from neurons with regard to prevailing expression of the long GlyR α3L RNA splice variant in neurons (Eichler et al., 2009).

Characteristics of GlyR expression in mouse GL261 glioma cells

We used here the EGFP-expressing mouse cell line GL261 (Walzlein et al., 2008), which is commonly used for the generation of experimental brain tumors in mice. GL261 cells selectively express mRNA coding only for the GlyR α1ins RNA splice variant (Malosio et al., 1991), and not for α2, α3, α4 or β subunits (Fig. 2A). To confirm that GlyR α1ins-coding mRNA results in expression of receptor protein, we used a polyclonal GlyR α1-directed antibody for immunochemical analysis of GL261 cells (Fig. 2B). Strong GlyR α1 protein expression was found in 10%±5 (±s.d., $n=3$ experiments) of GL261 cells. We verified that polyclonal GlyR α1 antibody-dependent signals were specific as evidenced by the congruency of immunochemical signals generated in combination with the well-characterized GlyR α1-specific mAb2b antibody (Fig. 2C). The GlyR α1-positive cells showed morphological peculiarities, such as a spherical shape and reduced adherence (Fig. 2B,C). More strikingly, GlyR α1 protein was detected mainly in the cytosol and nucleus of GL261 cells (Fig. 2B, right-hand high-power view, arrows; supplementary material Table S3), suggesting that GlyRs do not serve as neurotransmitter receptors in these cells. Consistent with the nuclear localization of GlyR α1, GL261 cells expressed importin α3 and α4 mRNA (Fig. 2D), which mediate nuclear import of GlyRs (Melzer et al., 2010).

GlyRs do not form glycine-gated ion channels at the surface of GL261 or human glioma cells

We used the patch-clamp technique to record membrane currents in response to glycine application. To monitor changes in membrane conductance, the membrane potential was repetitively clamped to a series of hyper- and de-polarizing potentials ranging from −120 to +20 mV, as described previously for the recording of γ-aminobutyric acid type A receptor ($GABA_AR$)-dependent Cl^- currents (Labrakakis et al., 1998). GlyR α1-positive, round shaped and slightly detached GL261 cells were investigated (Fig. 3A), but the membrane conductance was not affected by glycine application (Fig. 3B,C; $n=15$). Likewise, human glioma cells from resected glioblastoma multiforme did not respond to glycine application (TU7/00, supplementary material Fig. S1A, Fig. S3C; $n=15$), despite expression of GlyR α1- and α3-encoding mRNA in these cells (supplementary material Fig. S1B–D). GlyR α2-encoding mRNA was not detected (supplementary material Fig. S1D), whereas GlyR α4- and β-encoding mRNAs were expressed (supplementary material Fig. S1E). However, these GlyR

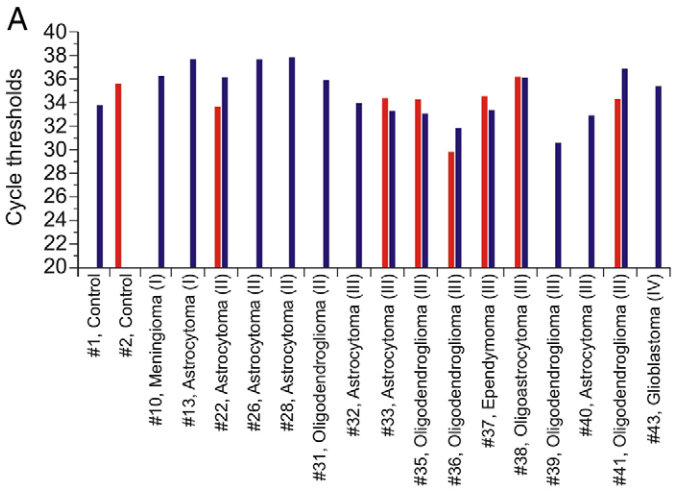

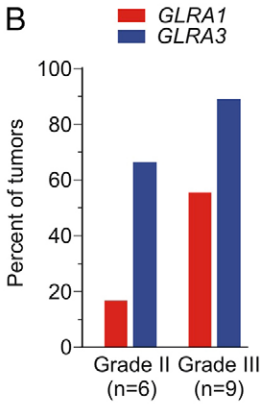

Fig. 1. GlyR α1 and α3 mRNA expression in human brain tumor biopsies. (A) Quantitative real-time PCR was performed to determine amplification cycle thresholds of mRNA coding for *GLRA1* (GlyR α1, red bars) or *GLRA3* (GlyR α3, blue bars) in human brain tumor biopsies. Low and high cycle threshold values indicate strong and weak gene expression levels, respectively. WHO tumor grading is indicated in brackets. (B) Quantification of the percentage of WHO grade II and III gliomas with *GLRA1* (red bars) and *GLRA3* (blue bars) gene expression. Details on brain tumor biopsies are provided in supplementary material Table S1.

Journal of Cell Science (2014) 127, 3687–3698 doi:10.1242/jcs.146662

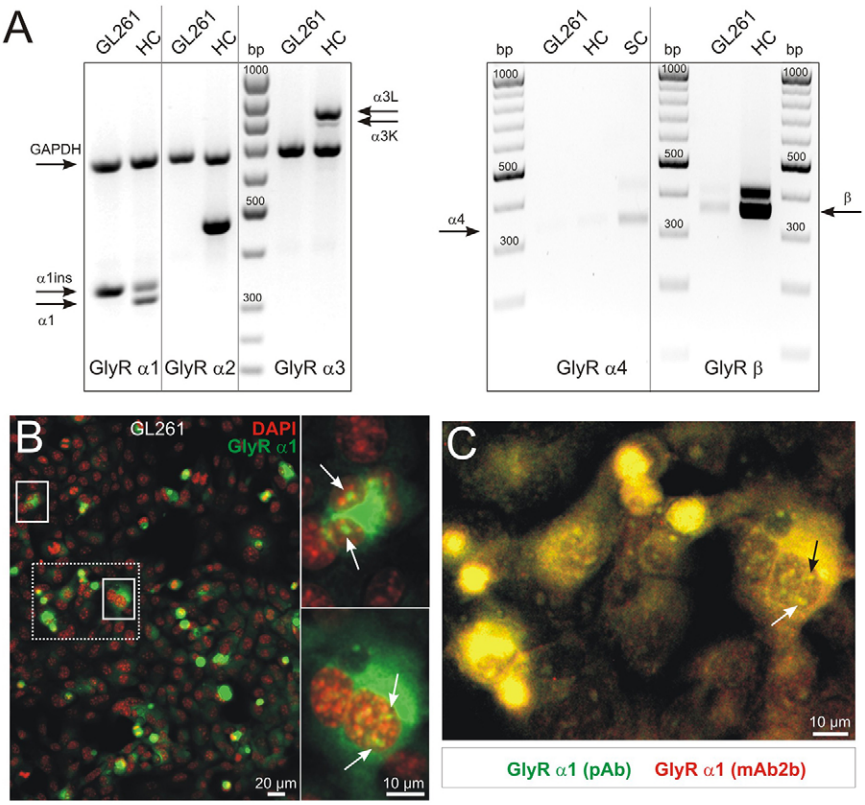

Fig. 2. GlyR α1 and importin expression in mouse GL261 cells. (A,B) Mouse GL261 glioma cells were processed for RT-PCR with oligonucleotides specific to GlyR α1, α2, α3, α4, and β cDNAs. For the GlyR α1 and α3 subunits, PCR products span alternatively spliced regions in the large cytosolic loop domain. To verify presence of mRNA, cDNA coding for the house keeping gene *GAPDH* was co-amplified. Furthermore, as a positive control, mRNA samples obtained from adult mouse hippocampus (HC) or spinal cord (SC) were included. Note that GL261 cells expressed only the 'ins' RNA splice variant of the GlyR α1 subunit. A faint band corresponding to GlyR β was also detected in the GL261 sample. (B,C) Immunochemical analysis of GlyR α1 protein expression in GL261 cells using a polyclonal antibody (B,C) and the well-characterized mAb2b antibody (C). Nuclei were visualized using DAPI stain (B). High-power views of the boxed regions are shown on the right (solid boxes) and in C (dashed box) and indicate intranuclear GlyR α1 expression (arrows; see supplementary material Table S3 for values). Also note that the immunochemical GlyR α1 signals obtained with two different antibodies are nearly congruent (C). (D) GL261 cells also expressed importin α3 and α4.

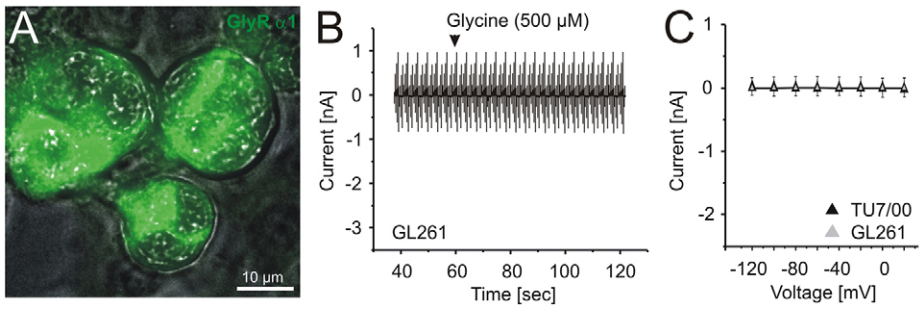

Fig. 3. Neither human nor mouse glioma cells respond to glycine application with transmembrane Cl^- currents. (A,B) GlyR α1-positive, typically round-shaped, glioma cells (A, example shown for GL261 cells) were selected for patch-clamp analysis. (B) Current profile of an example trace obtained from a round-shaped GL261 cell upon voltage ramps. The arrow marks the onset of glycine application (500 µM). (C) Summary of the current–voltage relationships obtained from recordings of mouse GL261 cells and human GlyR α1- and α3-expressing glioma cells (TU7/00, supplementary material Fig. S1) demonstrating failure of glycine application to induce transmembrane Cl^- currents.

Journal of Cell Science

Journal of Cell Science (2014) 127, 3687–3698 doi:10.1242/jcs.146662

subunits will not form functional neurotransmitter receptors at the cell surface of human cells. Thus, despite expression of various ligand-binding α-subunits, which are principally able to generate surface neurotransmitter receptors in human cells, GlyRs do not fulfill this task in mouse or human glioma cells (Fig. 3C). Furthermore, we found that importin α3 and α4 were expressed in the majority of samples derived from glioblastoma multiforme (supplementary material Fig. S1E), suggesting that GlyR subunits with NLSs (α1 and α3) have an intranuclear function in mouse and human glioma cells.

Full-length GlyR α1ins is expressed in intracellular compartments of glioma cells

Ubiquitin-dependent proteolytic processing of GlyR α1ins has been shown to release receptor fragments with molecular masses of 35 and 13 kDa, the latter corresponding to the size of large cytosolic loop including transmembrane domain (TM) 4 (Büttner et al., 2001). Hence, we next investigated whether proteolysis is responsible for intracellular GlyR expression in glioma cells (Fig. 4). To this end, we generated a recombinant GlyR α1ins expression construct with two different epitope tags located in the surface-accessible ligand-binding domain (Fig. 4A, Myc tag) and in the large cytosolic loop domain between transmembrane segments TM3 and TM4 [Fig. 4A, hemagglutinin (HA) tag]. We did not detect receptor protein fragments using an HA-directed antibody in western blot analysis (Fig. 4B). In agreement with the electrophysiological data shown above (Fig. 3), transfected GL261 cells did not show receptor surface labeling, although immunoreactivity of the HA epitope tag clearly revealed recombinant GlyR protein expression in the cytosol and nucleus (Fig. 4C; supplementary material Table S3). For control purposes, we verified that the recombinant GlyRs were able to access the cell surface in HEK293 cells (Fig. 4D). These results show that full-length GlyR α1ins is retained in intracellular compartments of glioma cells including the nucleus (supplementary material Table S3).

GlyR sequence-intrinsic determinants govern intracellular receptor expression

GlyR α1 and α3 subunits contain functional NLSs (RRKRR and RRKRK, respectively) in the large cytosolic loop domain (Melzer et al., 2010; Winkelmann et al., 2014). In the GlyR α2 subunit, the NLS is disrupted by insertion of glutamine residue (RRR**Q**KR, Fig. 5A). Furthermore, the GlyR α1 and α3 loops contain a di-leucine motif involved in adaptor protein 2 (AP2)-dependent receptor internalization (Huang et al., 2007) upstream of the NLS. In GlyR α2, the di-leucine motif is absent (Fig. 5A). To find out whether the NLS or the di-leucine motif is responsible for intracellular GlyR expression, recombinant GlyR α2 and chimeric GlyR α1–α2 constructs were generated and expressed in GL261 cells (Fig. 5B–D). Whereas GlyR α2 accessed the surface of transfected GL261 cells (Fig. 5B, Myc), disruption of the di-leucine motif by inserting the corresponding GlyR α2 sequences into GlyR α1 (myc-α1ins-NLS-ΔLL-α2-HA, Fig. 5A) was not sufficient for receptor surface expression (Fig. 5C). However, GlyR α1ins was detected at the cell surface, and it disappeared from the nucleus, upon additional disruption of the NLS (myc-α1ins-ΔLL-ΔNLS-α2-HA, Fig. 5A,D; supplementary material Table S3), suggesting that the NLS is responsible for the restriction of GlyR α1ins to the intracellular compartment of GL261 cells.

To investigate whether intracellular GlyR expression in GL261 is subunit specific or valid for all α-subunits with NLSs, we transfected GL261 cells with a mCherry–GlyR-α3K fusion construct and performed 3D confocal live-cell receptor imaging to further gather information about the dynamics of intracellular receptor distribution (supplementary material Movies 1–3; Fig. 6). Supplementary material Movies 1 and 2 show two views of the same cell (top and side views). Supplementary material Movie 3 shows another cell. Projected *z*-stacks of mCherry and Hoechst 33342 fluorescent signals (red and blue, respectively) acquired during 90-min recording intervals (supplementary material Movies 1–3; 30 frames/s with each

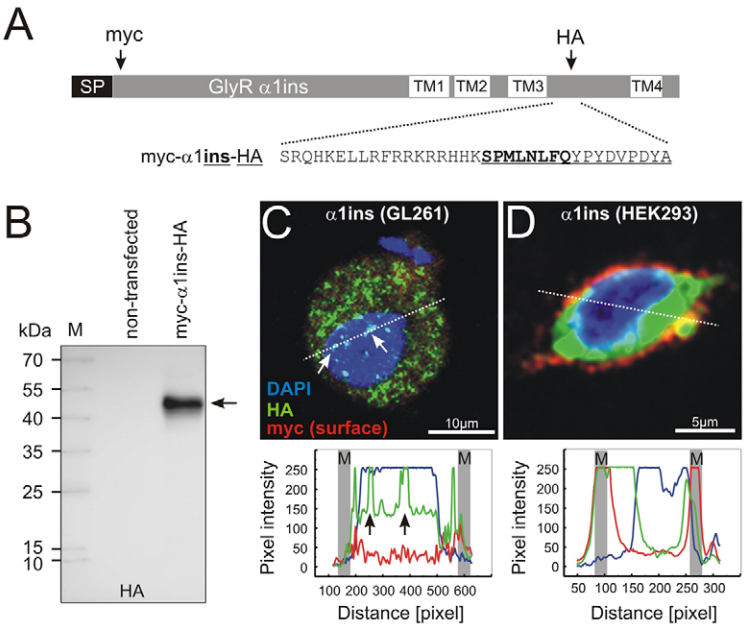

Fig. 4. Full-length GlyR α1 protein is expressed in cytosol and nucleus of GL261 cells. (A) Scheme depicting design of recombinant GlyR α1ins construct used for investigation of subcellular GlyR distribution, including the cell surface (using the Myc tag) and intracellular compartments (using the HA tag). Positions of the Myc and HA tags are marked with arrows. The zoomed region of the large cytoplasmic loop provides details on the amino acid sequence at the N-terminus of the large cytosolic loop. Sequence of the RNA splice insert 'ins' is highlighted bold and underlined, and the HA tag sequence is shown underlined. SP, signal peptide. (B) Western blot analysis of GlyR myc-α1ins-HA protein expression in non-transfected and transfected (myc-α1ins-HA) GL261 cells. A single band (arrow) corresponding to full-length (48 kDa) GlyR Myc–α1ins–HA protein was detected using the anti-HA antibody, ruling out proteolytic processing of GlyR α1ins in GL261 cells. M, molecular mass marker. (C) Confocal image of a GlyR myc-α1ins-HA-expressing GL261 cell. Note that surface accessible Myc tag was not detected using live-cell surface staining, whereas HA immunoreactivity (green) was detected in the cytosol and nucleus (blue) following cell fixation and permeabilization (see supplementary material Table S3 for values). GL261 cell nuclei are shown in blue color. Fluorescence profiles measured along the dashed lines are shown below the image. M, plasma membrane. (D) Confocal image of a GlyR myc-α1ins-HA-expressing HEK293 cell. GlyR myc-α1ins-HA was detectable at the cell surface, and HA immunoreactivity was found in cytosol but not nucleus. M, plasma membrane.

Journal of Cell Science (2014) 127, 3687–3698 doi:10.1242/jcs.146662

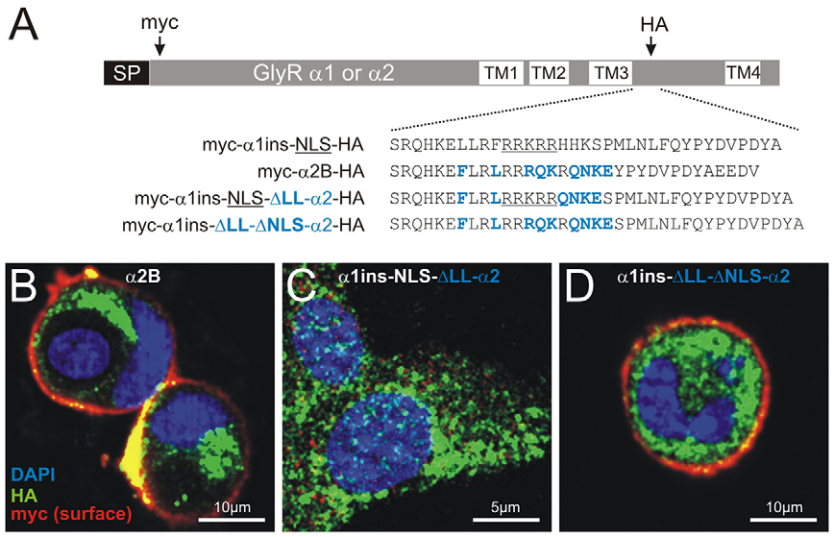

Fig. 5. The NLS region in the α1 subunit is responsible for intracellular GlyR expression in GL261 cells. (A) Scheme depicting design of recombinant GlyR α1ins or α2B constructs with a surface-accessible Myc tag, and a HA tag used for staining of the intracellular loop domain. The zoomed region provides details on the amino acid sequence at the N-terminus of the large cytosolic loop including the di-leucine motif up-stream of the NLS in GlyR α1ins (underlined). GlyR α2-specific sequence determinants are highlighted with blue color. In chimeric GlyR α1ins-α2, the di-leucine motif and NLS were disrupted by replacement of the corresponding amino acids in α1ins with those in α2 (blue). SP, signal peptide. (B–D) Confocal images showing immunochemical signals corresponding to the large cytosolic loop (HA tag, green) and the surface-accessible Myc tag (red) of representative transfected GL261 cells with GlyR myc-α2B-HA (B), myc-α1ins-NLS-ΔLL-α2-HA (C) or myc-α1ins-ΔLL-ΔNLS-α2-HA (D). GL261 cell nuclei appear in blue color. Live-cell surface staining with anti-Myc antibody revealed GlyR α2B expression at the GL261 cell surface (red). Note that GL261 cell nuclei were devoid of HA immunoreactivity. Also note that deletion of the di-leucine motif in GlyR α1ins was not sufficient to trigger receptor surface expression, whereas additional disruption of the NLS brought the subcellular distribution pattern of GlyR α1ins more in line with GlyR α2. See supplementary material Table S3 for quantification of nuclear versus somatic distribution of the recombinant GlyR constructs.

frame representing the projection of 10 *z*-sections, 1-μm step size) are shown. Individual frames extracted from supplementary material Movie 1 are shown in Fig. 6B and supplementary material Fig. S2. Besides the nuclear localization of GlyR α3K (supplementary material Table S3), the live-cell imaging also revealed that α3K clusters are highly mobile and rapidly shuttle back and forth between cytosol and nucleus (Fig. 6B, arrow, 00:14–00:16 min, and arrowheads, 00:19–00:20 min;

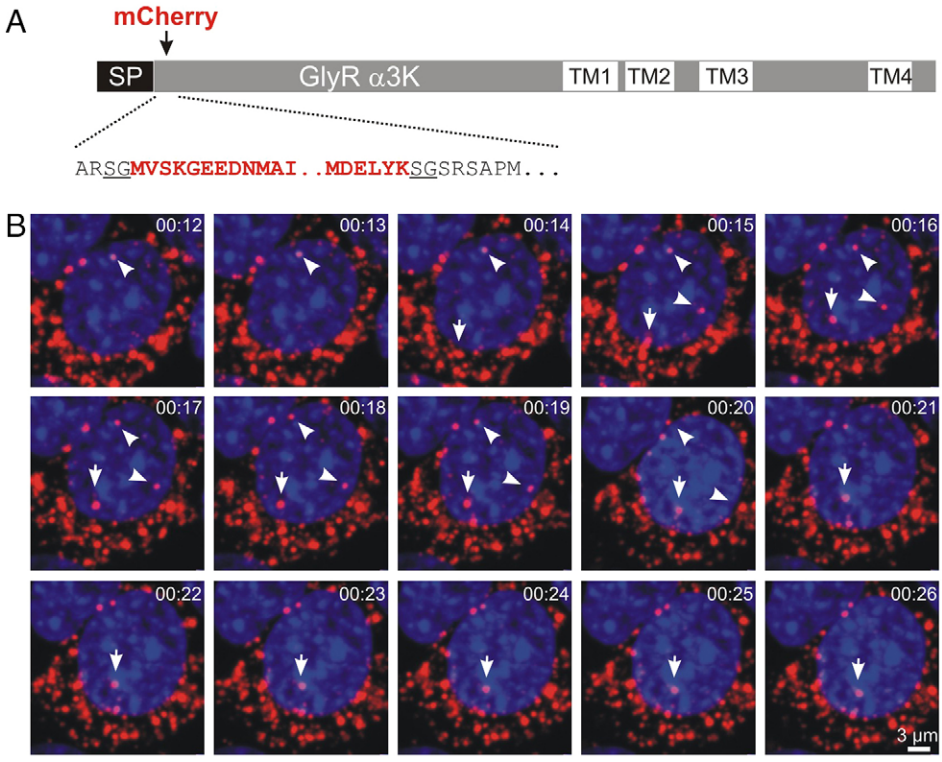

Fig. 6. GlyR α3 also targets to the nucleus of GL261 cells. (A) Scheme depicting design of recombinant GlyR α3K construct with N-terminal mCherry fluorescent protein used for confocal live-cell GlyR imaging. The zoomed region provides information on the position of mCherry fluorescent protein in GlyR α3K, which corresponds to the position of Myc tags in GlyR α1ins and α2B subunits, following the second amino acid of the mature signal-peptide-cleaved GlyR protein. Owing to insertion of the *BspE*1 cloning site, two additional amino acids (underlined) flank the mCherry sequence (red) in the mCherry–GlyR-α3K construct. SP, signal peptide. (B) Confocal images extracted from supplementary material Movie 1 providing information on the dynamics of intracellular mCherry–GlyR-α3K (red) distribution during a 15-min recording interval. Nuclei of GL261 cells appear in blue color. Note that α3K clusters enter (arrows) and exit (arrowheads) the nucleus within a minute, and that α3K clusters are associated with many sites inside GL261 cell nuclei. For a three-dimensional reconstruction of serial confocal images see supplementary material Fig. S2.

Journal of Cell Science (2014) 127, 3687–3698 doi:10.1242/jcs.146662

supplementary material Fig. 2B). Intra-nuclear dynamics, however, were much slower and α3K clusters remained associated with different euchromatin regions for several minutes (Fig. 6B, arrow). Just like GlyR α1ins (above, Fig. 4C), mCherry–GlyR-α3K clusters were thus detected at the same time at different euchromatin positions in the GL261 cell nucleus, suggesting that they might influence transcription of different genes. For control purpose, we verified that mCherry–GlyR-α3K accessed the surface of HEK293 cells by recording glycine-dependent transmembrane Cl^- currents (supplementary material Fig. S3). Collectively, these results show that the NLSs in the large cytosolic loops of full-length α1ins and α3K GlyRs mediate cytosolic and intra-nuclear receptor expression specifically in glioma cells.

Knockdown of GlyR expression changes GL261 gene expression

To study functional relevance of intracellular GlyR expression, GlyR α1ins expression was knocked down in GL261 cells. Stable knockdown cell lines were obtained by transfection of GL261 cells with GlyR α1-specific small hairpin RNA (shRNA) constructs 'G10' and 'G11' (Fig. 7A). Our immunochemical analyses confirmed the shRNA-dependent impact on GlyR α1 protein expression because ubiquitin-associated perinuclear GlyR α1 immunoreactivity was detected in G10 and G11 cells (Fig. 7B, α1-KD-1 and α1-KD-2). Consistently, the western blot analyses revealed that full-length GlyR α1ins protein expression was reduced to 36.3%±1.8 in α1-KD-1 and 13.4%±0.8 in α1-KD-2 cells (mean±s.d., $n=3$ experiments) compared to the expression level in control GL261 cells (set at 100%). Western blotting against the house-keeping protein α-tubulin served as reference for normalization purpose (Fig. 7C,D). To find out whether intra-nuclear GlyR expression changes gene expression in GL261 cells, we performed quantitative real-time PCR to compare mRNA expression of mouse orthologs of human genes selected by the International Stem Cell Initiative (Adewumi et al., 2007), using the Mouse Stem Cell Pluripotency Array. Reduced GlyR α1ins protein expression indeed affected the mRNA expression of many

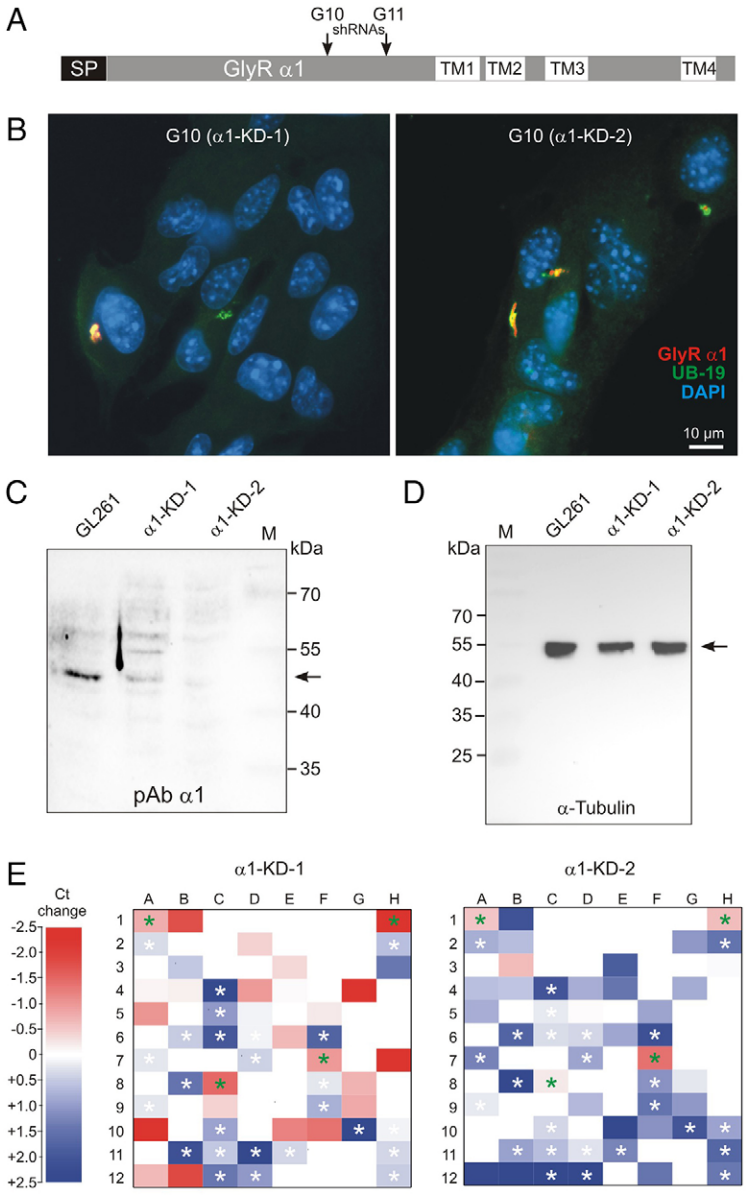

Fig. 7. Knockdown of GlyR α1ins expression changes gene expression in GL261 cells. (A) Scheme depicting position of hybridization of the two effective shRNAs, TRC6-G10 (G10) and TRC6-G11 (G11). (B) Immunochemical analysis of GlyR α1 distribution in G10- and G11-knockdown cells. Note that shRNA expression resulted in colocalization of GlyR α1 with ubiquitin (UB-19) in the perinuclear compartment. (C,D) Western blot analyses of GlyR α1 and α-tubulin protein in GL261 cells and the GlyR α1 knockdown cell lines α1-KD-1 and α1-KD-2. Bands corresponding to GlyR α1 (C) and α-tubulin (D) are marked with arrows. (E) The color code represents changes in cycle thresholds (Ct) compared to GL261 cells. Color-coded heat maps show downregulated gene products (blue squares) in both α1-KD-1 and α1-KD-2 GlyR α1ins knockdown GL261 cells. They are marked with white asterisks and mainly belong to the categories 'signaling pathways' (*Raf1*, *Gal*, *Grb7*), 'transcriptional and translational regulation' (*Eomes, Eef1a1, Gata4, Isl1, Olig2* and *Pax6*) and 'stemness' (*Bxdc2*, *Cd9*, *Dnmt3b*, *Gata6*, *Gdf3*, *Il6st*, *Kit*, *Ifitm2*, *Nes* and *Tert*). Upregulated gene products (red squares) were *18S*, *Gcg*, *Pax4* and *Tdgf1* (green asterisks).

Journal of Cell Science (2014) 127, 3687–3698 doi:10.1242/jcs.146662

different genes (Fig. 7E; supplementary material Table S4). Downregulated gene products in both α1-KD-1 and α1-KD-2 GlyR α1ins-knockdown cells included those involved in signaling pathways, including the extracellular-signal-regulated kinase (ERK) (*Gal*, *Grb7*, *Raf1*; Fig. 7E; supplementary material Table S4) and β-catenin/Wnt (proto-oncogene *Ctnnb1*) pathways. Furthermore, mRNA expression of transcriptional regulators (*Eomes*, *Eef1a1*, *Gata4*, *Isl1*, *Olig2*, *Pax6*) and factors that determine self-renewal capacity (*Bxdc2*, *Cd9*, *Dnmt3b*, *Gata6*, *Gdf3*, *Il6st*, *Kit*, *Ifitm2*, *Nes*, *Tert*) were downregulated in the two GlyR knockdown cell lines. Just a few gene products were upregulated (*Gcg*, *Pax4*, *Tdgf1*; Fig. 7E; supplementary material Table S4). These results show that intracellular GlyRs modify expression of genes with tumorigenic potential.

Knockdown of GlyR expression impairs neurosphere formation

To address the possibility that the GlyR-dependent impact on GL261 gene expression affects the self-renewal capacity of GL261 cell, we used the limiting dilution assay, which is an independent predictor of clinical outcome in malignant glioma (Laks et al., 2009). To this end, the different GL261 cell lines were cultured in stem cell medium until the first neurospheres appeared. Then, the minimal number of cells required for neurosphere formation in each well of the culture dish was determined (Fig. 8). A much higher number of the GlyR-knockdown cells as compared to control GL261 cells was required for sphere formation, indicating that neurosphere formation was suppressed in α1-KD-1 and α1-KD-2 cells

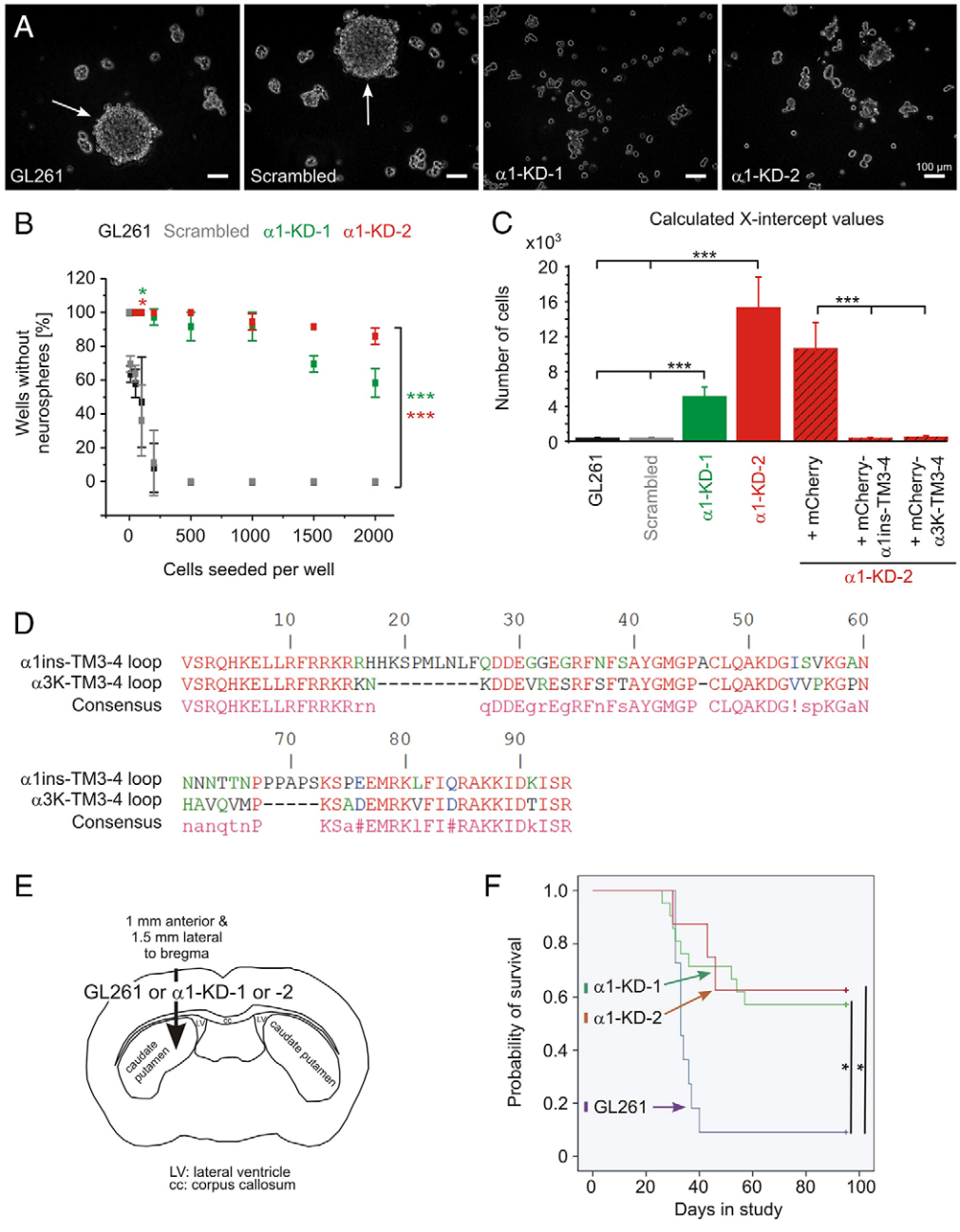

Fig. 8. Knockdown of GlyR α1ins expression impairs neurosphere and glioma formation. (A–C) For the limiting dilution assay and investigation of the neurosphere-forming capacity, GL261, scrambled shRNA-expressing GL261, α1-KD-1, α1-KD-2 cells, and α1-KD-2 cells expressing mCherry, mCherry-α1ins-TM3-4 or mCherry-α3K-TM3-4 were cultured in stem cell medium for 1 week. (A) Images show representative examples of neurosphere formation (arrows) in wells with 1000 seeded cells. (B) Quantification of the percentage of wells without neurospheres per cell plating density (10, 50, 100, 500, 1000, 1500 or 2000 cells per well). Note the strongly reduced sphere-forming capacity of α1-KD-1 or α1-KD-2 cells throughout all investigated cell plating densities. (C) Linear regression analysis was performed in order to determine the minimal number of cells per well required for formation of at least one neurosphere (*x*-intercept value). **P*<0.05 (100 cells), ****P*<0.001 (all cell plating densities except 100 cells per well), as determined by one-way ANOVA with post-hoc Bonferroni tests. (D) Sequence alignment of GlyR α1ins and α3K large cytosolic loops reveal a high degree of similarity. (E) Scheme providing information on stereotactic injection of GL261, α1-KD-1 or α1-KD-2 knockdown cells into the mouse brain. (F) Cumulative survival plot of mice that were inoculated with GL261, α1-KD-1, or α1-KD-2 knockdown cells. Note that knockdown of GlyR α1 expression strongly impaired glioma formation *in vivo* as both life span and survival rate of knockdown cell-inoculated mice were increased.

Journal of Cell Science (2014) 127, 3687–3698 doi:10.1242/jcs.146662

(Fig. 8B,C; *x*-intercept values, α1-KD-1, 5137±871, α1-KD-2, 15,800±2880 versus GL261 control cells, 249±61; mean±s.e.m.). As a control for the shRNA knockdown strategy, we verified that expression of scrambled shRNA did not influence the capacity of GL261 cells to form neurospheres (*x*-intercept value of scrambled shRNA-expressing GL261 cells, 247±78, mean±s.e.m.). Importantly, stable expression of the large cytosolic GlyR α1ins loop between TM3 and TM4 rescued the sphere formation capacity of α1-KD-2 cells (Fig. 8C, *x*-intercept value of mCherry–α1ins-TM3-4-expressing GL261 cells, 280±97; mean±s.e.m.), which clearly identifies the loop as the relevant GlyR α1ins signaling domain. Moreover, the large cytosolic GlyR α3K loop was equally effective in rescuing the self-renewal capacity of α1-KD-2 cells (Fig. 8C, *x*-intercept value of mCherry–α3K-TM3-4-expressing GL261 cells, 365±144, mean±s.e.m.). As a control, we verified that mCherry expressed without GlyR protein domains did not influence the capacity of GL261 cells to form neurospheres (Fig. 8C, *x*-intercept value of mCherry-expressing α1-KD-2 cells, 10,519±3420, mean±s.e.m.). Thus, reduced GlyR α1ins protein expression impairs the self-renewal capacity of GL261 cells. It is striking, that both GlyR α1ins and the α3K large cytosolic loops are able to rescue it and, hence, are two functionally equivalent versions of the relevant signaling domain (Fig. 8D).

Knockdown of GlyR expression impairs glioma formation *in vivo*

In order to find out whether impaired self-renewal capacity would result in reduced tumorigenicity, GL261, α1-KD-1 and α1-KD-2 cells were inoculated by stereotactic injection into the caudate putamen of GL261-isogenic wild-type mice (Fig. 8E), and the probability of survival and the lifespan of GL261-cell-inoculated mice were monitored (Fig. 8F). Reduction of GlyR α1ins protein expression impaired glioma formation *in vivo* as the majority of knockdown-cell-inoculated mice survived without developing tumors [Fig. 8F; 57% (12 of 21) of α1-KD-1-inoculated mice, and 63% (5 of 8) of α1-KD-2-inoculated mice]. Furthermore, the lifespan of knockdown-cell-injected mice with tumor formation was significantly prolonged, which suggests that glioma formation was slowed down in those animals that developed tumors despite knockdown of GlyR expression (Fig. 8F). Consistently, post-mortem analysis revealed similarly sized tumors in all animals which died due to GL261 cell inoculation (supplementary material Fig. S4A–C), but with a significant delay in the experimental mouse groups that were inoculated with GlyR-knockdown cells (Fig. 8F). Thus, we also conclude that knockdown of GlyR α1ins expression impairs tumor progression *in vivo*, which is supported by reduced proliferation rates of α1-KD-1 and α1-KD-2 cell lines in cell culture (supplementary material Fig. S4D). Collectively, these results identify a crucial role of intracellular GlyR function for regulation of tumorigenicity and tumor progression.

DISCUSSION

The neurotransmitter glycine has been shown to serve a metabolic role in brain tumor formation (Jain et al., 2012). The high glycine content of brain tumors (Bobek-Billewicz et al., 2010) prompted us to test whether glioma cells express GlyRs to sense the glycine level in the extracellular space. We found, however, that NLS-harboring receptors were not expressed on the cell surface, but rather served a new intracellular signaling function that modified tumor cell gene expression, self-renewal capacity and tumorigenicity.

Mouse GL261 glioma and human stem-cell-like tumor cells preponderantly expressed the GlyR α1ins and α3K RNA splice variants, which contain the sequence SPMLNLFQ (Malosio et al., 1991) and lack the splice insert coding for TAEFALEKFYRFSDT (Nikolic et al., 1998), respectively. The protein region where RNA splicing changes amino acid sequences is interesting as it is located immediately downstream of the NLS region. It has been established that this protein region influences GlyR protein structure as, for example, inclusion of exon 8A (coding for TAEFALEKFYRFSDT) changes receptor desensitization kinetics, clustering and subcellular trafficking in neurons (Eichler et al., 2009; Nikolic et al., 1998; Notelaers et al., 2012; Winkelmann et al., 2014). The tumor-cell-specific preponderant expression of GlyR α1ins and α3K RNA splice variants identifies a functional role for GlyR α1ins and sets glioma cells apart from neurons with regard to RNA splicing of GlyR α3-coding gene transcripts (Eichler et al., 2009). Our results also identify a possible crucial functional role for non-charged amino acids corresponding to the RNA splice insert downstream of the NLS in GlyR α1.

Although it has been established that the monopartite NLS in the large cytosolic GlyR loop domain is able to interact with nuclear import proteins of the karyopherin family (importin α3 and α4) (Melzer et al., 2010), the functional impact of the NLS in GlyR α1 and α3 subunits remained elusive. Western blot analyses of GlyR-transfected GL261 cells revealed that nuclear GlyR expression was not due to release of GlyR protein fragments upon proteolysis. This is distinct to other transmembrane receptors, which are known to require release of proteolytic protein fragments for activation of intracellular signaling domains (Hollmén et al., 2012; Nanba et al., 2003). Our experiments with chimeric GlyR constructs furthermore showed that deletion of the di-leucine motif involved in receptor internalization (Huang et al., 2007) was not sufficient to change the subcellular receptor distribution in GL261 cells. In support of a crucial role for the NLS region, additional deletion of the NLS in GlyR α1 was sufficient to enable receptor surface expression in GL261 cells. Although we cannot rule out a possible contribution of the β subunit (Fig. 2A; supplementary material Fig. S1E) to the peculiar subcellular GlyR trafficking in glioma cells (Del Pino et al., 2014), our data present evidence for a crucial role of the NLS region in the intracellular GlyR function discovered in this study.

In agreement with the established membrane topology of full-length GlyRs (Breitinger and Becker, 2002; Zuleger et al., 2012), the large cytosolic loop domain between transmembrane segments 3 and 4 of intranuclear GlyRs will be exposed to genomic DNA in the nucleoplasm of glioma cells. In fact, Cys-loop neurotransmitter receptors have a common origin (Tasneem et al., 2004), and our BLAST search of the NCBI prokaryote database revealed substantial (~30%) similarity between the large cytosolic GlyR loop domain encoded by exon 9 and prokaryotic proteins with molecular chaperone function (proteasome-activating nucleotidase, sequence ID: gb|ADD93104.1) or DNA-processing activity (type III restriction protein res subunit, sequence ID: gb|EMA60229.1). Furthermore, we recently presented evidence for co-sedimentation of GlyR large cytosolic loops with RNA-binding proteins and proteins that regulate transcription [e.g. heterogeneous nuclear ribonucleoprotein K (*Hnrpk*) or transcriptional activator protein Purα (*Pura*) (see Winkelmann et al., 2014)]. In agreement with an evolutionarily conserved role of exons in exon-shuffled contemporary genes in mammals, it is tempting to speculate that

the functional impact of NLS-harboring GlyRs in glioma cells involves regulation of gene expression. Our quantitative PCR analysis of the Mouse Stem Cell Pluripotency Array (Adewumi et al., 2007) indeed supports this idea as it identified a set of GlyR target genes. Most of them belong to the category 'stemness' (*Bxdc2*, *Cd9*, *Dnmt3b*, *Gata6*, *Gdf3*, *Il6st*, *Kit*, *Ifitm2*, *Nes*, *Tert*) and are good candidates for the genes that are responsible for the impaired self-renewal capacity of α1-KD-1 and α1-KD-2 cells in the neurosphere formation assay and the reduction in the initiation of glioma formation by GlyR α1ins knockdown GL261 cells in the experimental mouse model. Although the exact signaling mechanisms of the GlyR-dependent impact on GL261 gene expression remain to be determined, our study identifies an intriguing strategic (possibly gene regulatory) role for the NLS-harboring large cytoplasmic loop domain of GlyRs in glioma cells. That both GlyR α1ins and α3K large cytosolic loop domains were able to rescue self-renewal capacity of GlyR α1ins knockdown GL261 cells indeed demonstrates functional equivalence of these protein domains. In fact, the large cytosolic loops of GlyR α1ins and α3K share 60% sequence similarity (Combet et al., 2000). Thus, the identified GlyR protein regions and their consensus sequence (Fig. 8D) might be relevant for tumor therapy as they could be functionally neutralized using cell-penetrating peptides that specifically target glioma cells through proteolytic activation (Jiang et al., 2004) in patients with GlyR α1- and/or α3-positive brain tumors.

In summary, our study determines the GlyR α1ins and α3K large cytosolic loops as glioma-cell-specific and tumorigenic intracellular receptor signaling domains. These results make a strategic contribution to the field by revealing a new intracellular and gene regulatory GlyR function that goes much beyond the well-established role of the protein as a neuronal Cys-loop neurotransmitter receptor.

MATERIALS AND METHODS

Analysis of resected brain tumors was performed according to the rules laid down by the Ethical Committee (Charité, EA4-098-11), and informed consent was obtained according to the Declaration of Helsinki (2000). Animals were treated according to the permit given by the Office for Health Protection and Technical Safety of the regional government of Berlin (LaGeSo, TVV 230/05), in compliance with regulations laid down in the European Community Council Directive.

GlyR expression constructs

Recombinant GlyR α1ins and α2B expression constructs with surface accessible Myc and intracellular HA epitope tags were generated using site-directed mutagenesis, following the GeneEditor protocol (Promega, Mannheim, Germany). The Myc tag was inserted between the second and third amino acid of the mature, signal peptide cleaved, receptor proteins. The mCherry–GlyR-α3K construct for confocal live-cell imaging was obtained likewise by inserting a *BspE*1 restriction site at this position and in-frame cloning of mCherry-coding sequence. To generate GlyR mCherry–α1ins-TM3-4 and mCherry–α3K-TM3-4 loop constructs for the production of Zeocin-resistant stable cell lines, standard molecular cloning procedures were used for their cloning into the pTRACER vector (Clontech). In fusion constructs, the loop domains started with 'VSK' and ended with 'ISR' followed by linker 'GPVAT' (α1ins) or 'PVAT' (α3K) and the mCherry-coding sequence. In addition, because GL261 cells already express EGFP, the EGFP-coding sequence in the Zeocin-resistance cassette was excised using fusion PCR. Corresponding cDNA clones (Legendre et al., 2009) served as PCR templates. All constructs were verified by DNA sequencing.

Resected brain tumors and cell lines

Resected brain tumors were provided by the Department for Neurosurgery Charité Universitätsmedizin Berlin. Brain tumor material for RT-PCR analysis of GlyR expression was obtained from four patients (TU4/01, primitive neuroectodermal tumor; TU3/01, TU4/06 and TU7/00, glioblastoma multiforme, WHO grade IV), and corresponding cell lines were produced by culturing the dissociated tumor cells in Dulbecco's Modified Eagle Medium (DMEM; #41965, Invitrogen Life Technologies, Carlsbad, CA) supplemented with 10% FCS, 2 mM L-glutamine, 100 U/ml penicillin and 100 µg/ml streptomycin at 37℃ and under 5% CO_2, as described previously (Labrakakis et al., 1998). The EGFP-expressing high-grade astrocytoma cell line GL261 (Walzlein et al., 2008) (which is isogenic to C57BL/6 mice; National Cancer Institute, Frederick, MD) was used throughout and cultured as shown above or in stem cell medium [2% B27, 100 U/ml penicillin, 100 µg/ml streptomycin, 20 ng/ml FGF-2, 20 ng/ml EGF in DMEM supplemented with F-12 (Invitrogen Life Technologies)].

Transfection of GL261 cells was carried out using an Amaxa Nucleofector system (kit V, program V001; Lonza, Basel, Switzerland). GlyR α1-knockdown cell lines were obtained by electroporation of 3×10^6 to 5×10^6 GL261 cells with 2 µg of the shRNA expression constructs directed against GlyR α1 (TRC6-G10 and TRC6-G11) or containing scrambled shRNA sequences (Open Biosystems, Huntsville, AL), as a control. To select and maintain stable shRNA-expressing GL261 cells, 0.8 µg/µl puromycine was added to the culture medium. Two stable GlyR α1 knockdown cell lines were obtained with shRNAs TRC6-G10 and TRC6-G11, which are referred to here as α1-KD-1 and α1-KD-2. Stable α1-KD-2 cell lines expressing mCherry, or constructs encoding the mCherry–α1ins-TM3-4 loop or the mCherry–α3K-TM3-4 loop were obtained following nucleofection using program U030 and selection with additional Zeocin antibiotic at a concentration of 300 µg/ml. mCherry fluorescence was monitored throughout the experiments (not shown). For immunocytochemistry, GL261 cells were transfected with GlyR-coding plasmids using the Amaxa Nucleofector system as described above, but applying the program U020. Transfection of GL261 with the mCherry–GlyR-α3K construct for confocal live-cell imaging was conducted with magnefect-nano (0.24 µg DNA, 0.82 µl nano particles, 1 Hz, 0.2 mm displacement, 1 h; nanoTherics Ltd, Keele, UK). For this purpose, cells were seeded in 24-well plates at an initial cell density of 30,000 cells per well 1 day before transfection, dissociated with trypsin and re-seeded at 1:1 into 35-mm glass-bottomed microwell dishes (MatTek, Ashland, MA) at 1 day post transfection. Live-cell imaging was performed at 4 days post transfection.

Human embryonic kidney cells (HEK293) were cultured as described above and transfected using a standard Ca^{2+}/phosphate protocol. At 2 to 3 days after transfection, cells were processed for electrophysiology, immunochemistry or live-cell imaging.

Neurosphere formation in the limiting dilution assay

For the limiting dilution assay, cells were cultured in stem cell medium until primary sphere formation was noted. Cells were then dissociated and plated in 96-well plates in 0.2 ml volumes of stem cell medium. Final cell dilutions ranged from 2000 cells/well to 10 cells/well in 0.2 ml volumes. Twelve wells were seeded per cell plating density. Cultures were fed 0.025 ml of stem cell medium every 2 days until day 7, when the percentage of wells not containing spheres for each cell plating density was calculated and plotted against the number of cells per well. Regression analysis was performed to extract *x*-intercept values, which represent the number of cells required to form at least one neurosphere in every well.

Inoculation of GL261 cells into the mouse brain

Female wild-type C57Bl/6 mice were purchased from Charles River Laboratories (Sulzfeld, Germany) or bred at the local animal facility. Mouse GL261 control or GlyR α1-knockdown cells (α1-KD-1 and α1-KD-2) were suspended in MEM Eagle with Earle's BSS supplemented with vitamin B12 (0.25 µM) and B27 supplement (20 µl/ml; both Invitrogen), and 1 µl of cell suspension ($2*10^4$ cells/µl) was injected into

Journal of Cell Science (2014) 127, 3687–3698 doi:10.1242/jcs.146662

the caudate putamen region (1 mm anterior and 1.5 mm lateral to the bregma, as described previously (Glass et al., 2005).

Electrophysiology

For patch-clamp experiments, extracellular and intracellular solutions were as described previously (Labrakakis et al., 1998). Briefly, extracellular solution contained (in mM) NaCl (150), KCl (5.4), HEPES (5), glucose (10), $CaCl_2$ (2) and $MgCl_2$ (1). The pH was adjusted to 7.4 with KOH. Patch pipettes were pulled from a borosilicate glass tube (Hilgenberg GmbH, Malsfeld, Germany) with a horizontal puller (Sutter Instruments, Novato, CA), electrode resistance was 6–8 MΩ. Pipette solution contained (in mM) KCl (130), EGTA (5), HEPES (10), $CaCl_2$ (0.5), $MgCl_2$ (2) and ATP (3). Patch-clamp experiments were performed at room temperature. Membrane current recording and voltage stimulation were performed with a patch-clamp amplifier (EPC9 or EPC9/2, HEKA Elektronik, Lambrecht, Germany) and traces were acquired with a 3.0 kHz Bessel filter. Bath application of a nearly saturating glycine concentration (500 µM) was performed 30 s after the baseline current at the holding potential of −60 mV had stabilized. To obtain current voltage curves, the membrane was clamped to a series of depolarizing and hyperpolarizing voltage steps from the holding potential (−120 mV to +20 mV, step size: 20 mV, step duration: 200 ms, duration between steps: 300 ms). In each set of experiments we compared the inward currents prior to glycine application with the ones recorded 15 s after glycine application. The latter corresponds to the time point at which glycine-evoked responses usually peaked in GlyR α1-transfected HEK293 control cells. Average conductance was calculated by linear interpolation of voltage steps between −120 mV and +20 mV. For patch-clamp recording of HEK293 cells, extracellular solution contained (in mM) NaCl (140), KCl (5), HEPES (10), glucose (10), $CaCl_2$ (2), and $MgCl_2$ (1). The pH was adjusted to 7.4 with NaOH. Patch pipettes were pulled from a borosilicate glass tube (1B150F-4; World Precision Instruments, Berlin, Germany) with a horizontal puller (Sutter Instruments, Novato, CA), and had resistances of 3–6 MΩ when filled with internal solution. Pipette solution contained (mM) CsCl (130), NaCl (5), $CaCl_2$ (0.5), $MgCl_2$ (1), EGTA (5) and HEPES (30), pH was adjusted to 7.2 with CsOH. Cells were clamped at −50 mV and current–voltage (*I–V*) relations were obtained from voltage ramps from −100 mV to +100 mV with a duration of 400 ms applied every 5 s. Traces were recorded with a List EPC7 amplifier and Patchmaster software. Data were sampled at 10 kHz and filtered online at 2.83 kHz (10 kHz + 3 kHz Bessel). HEK cells (500,000) were seeded onto 35-mm dishes 3 days before, and transfected 1 day before measurement with 2 µg plasmid DNA (containing either mCherry-GlyRα3K) and Fugene HD® (Promega, Mannheim, Germany) according to the manufacturer's instructions. At 1–5 h prior to the recording, transfected HEK293 cells were split 1:6 onto glass coverslips and identified according to mCherry fluorescence, which was acquired under a 40× objective using a 16-bit cooled CCD camera (Spot PURSUIT, Visitron Systems GmbH, Puchheim, Germany).

RNA isolation, cDNA synthesis and PCR

RNA was isolated from cultured cells using TRIzol Reagent (Invitrogen). cDNA was obtained by reverse transcription of 2 µg RNA with an equimolar mixture of 3′-anchored poly(T) oligonucleotides ($T_{18}V$, $T_{15}V$, $T_{13}V$) and Superscript II (Invitrogen), according to the manufacturer's protocol.

For PCR amplification of cDNA obtained from human glioma cells, oligonucleotides binding to specific sequences of GlyR α1 (5′-CAGTTTGCCTGCTCTTTGTGT-3′ and 5′-GTTGAAAATGAGGAAGGCCATG-3′), α2 (5′-ATCAACAGTTTTGGATCAGTCA-3′ for the α2A splice variant or 5′-TCAACAGCTTTGGGTCAATAG-3′ for α2B and 5′-CCTTCAGCAACTTGCACTGG-3′ for both) and α3 (5′-GGGTACACAATGAATGATCTC-3′ and 5′-AGAGACTTAATCTTGCTGCTGATG-3′) were designed as described previously (Eichler et al., 2008; Eichler et al., 2009; Meier et al., 2002) and used in combination with GAPDH-specific primers (5′-ATGGCACCGTCAAGGCTGAG-3′ and 5′-CGACGCCTGCTTCACCACC-3′) (Eichler et al., 2009). The ratio between GlyR α- and GAPDH-specific oligonucleotides was adjusted to 15:1 (α1 and α2) and 20:1 (α3). For detection of the α4 subunit, oligonucleotides 5′-AGCATAAAGAATTCATACGACTTCGA-3′ and 5′-TGGATATCTTCTGACCATAGCACT-3′ were used. The β subunit was detected using oligonucleotides 5′-TGAGCAAGCAGATGGGAAAGG-3′ and 5′-TAACGTTGAAGAACAAGAAGCAG-3′. Specific oligonucleotides were used for detection of importin α3 (5′-GATGGTTATTGATTCAGGGGTTGTAC-3′ and 5′-GATGAATAATCATAGGGATTAACCCA-3′) and importin α4 (5′-GATGGTAATAGACTCTGGCATAGTTC-3′ and 5′-GGTGTATTATCATTGGTACAAGATTG-3′). RedTaq DNA polymerase (Sigma-Aldrich, Deisenhofen, Germany) and manual hot start were applied, and 40 cycles (1 min annealing at 58℃ and 1 min elongation at 72℃) were run. For the purpose of control of oligonucleotides and the PCR protocol, human post-mortem hippocampus RNA (pool of 20 healthy Caucasians) was purchased from Clontech and included in PCR.

cDNA of mouse GL261 glioma cells was screened as described above, except that oligonucleotides specific to mouse GlyR α1 (5′-CTGTTTGCCTGCTCTTCGTGT-3′ and 5′-TGGGGAAACCGATGCGAGATA-3′), α2 (5′-ACCGAGTGAATATTTTTCT GAGAC-3′ and 5′-GTGAAACTTGACCTCAATGCAG-3′), α3 (5′-GGGTACACAATGAATGATCTC-3′ and 5′-AGAGACTTAATCTTGCTGCTGATG-3′), α4 (5′-AGCATAAGGAATTTATGAGACTTCGA-3′ and 5′-TGGATATCTTCTGACCTTAGTACT-3′), β (5′-TGAGCAAGCAGATGGGAAAGG-3′ and 5′-TAACGTTGAAGAACAAGAAGCAG-3′), importin α3 (5′-GATGGTTATTGATTCAGGGGTTGTAC-3′ and 5′-GATGAATAATCATAGGGATTAACCCA-3′) and importin α4 (5′-GATGGTAATAGACTCTGGCATAGTTC-3′ and 5′-GGTGTATTATCATTGGTACAAGATTG-3′) were used. GAPDH-specific primers (5′-CCACTCACGGCAAATTCAACG-3′ and 5′-AGCCCAAGATGCCCTTCAGTG-3′) were included, and again, the ratio between GlyR α- and GAPDH-specific oligonucleotides was adjusted to 15:1 (α1 and α2) and 20:1 (α3). A total of 35 cycles (1 min annealing at 54℃ and 1 min elongation at 72℃) were run. For the purpose of control of oligonucleotides and the PCR protocol, adult mouse hippocampus RNA was processed accordingly.

Quantitative real-time PCR, human brain cancer tissue and the mouse stem cell pluripotency array

A β-actin-normalized cDNA panel of pathologist-verified human brain tumors (OriGene Technologies, Inc., Rockville, MD, USA) was used to probe for *GLRA1*, *GLRA2*, and *GLRA3* gene transcript levels by quantitative real-time PCR. The following TaqMan Gene Expression Assays (Applied Biosystems, Foster City, CA, USA) were used: GLRA1_Hs00609267_m1, GLRA2_Hs01033736_m1 and GLRA3_Hs00197920_m1. Quantitative real-time PCR was performed according to the TaqMan Gene Expression Assay protocol using the iCycler IQ 5 multicolor real-time detection system (Bio-Rad, Munich, Germany). cDNAs obtained from GL261 control or GlyR α1 knockdown cells (α1-KD-1 and α1-KD-2) were analyzed in a TaqMan Mouse Stem Cell Pluripotency Array (Invitrogen #4414080) using a 7500 real-time PCR system with SDS Software and TaqMan universal PCR master mix (Applied Biosystems, Foster City, CA, USA) according to the manufacturer's instructions. Data were acquired for 40 cycles (cut-off).

Western blotting

Western blot was performed for verification of GlyR protein expression in GL261 cells and quantification of GlyR α1 knockdown in α1-KD-1 and α1-KD-2 cells. Cells were homogenized in the presence of lysis buffer (1% CHAPS, 10 µM pepstatin, 10 µM leupeptin, 0.52 µM aprotinin and 200 µM PMSF in PBS) and centrifuged for 15 min at 4℃ and full speed (16,100 ***g***). The protein concentration was determined using the Warburg–Christian equation $[1.55\times(A_{280}-A_{320})-0.76\times(A_{260}-A_{320})]$, where A is the absorbance at the given wavelength, after measuring the extinction with a standard Eppendorf BioPhotometer. Proteins were supplemented with 5× SDS sample buffer containing 50% glycerol, 3.5% SDS, 15% β-mercaptoethanol and 0.02% Bromphenol Blue and boiled for 7 min at 95℃. A total of 8 µg protein per lane was loaded on a 10% SDS gel and run for 1 h at 35 mA (Mini-PROTEAN Tetra System,

Bio-Rad Laboratories, Hercules, CA). Proteins were blotted on a nitrocellulose membrane (0.45 µm, Bio-Rad Laboratories) for 1 h at 2 mA/cm^2. After blotting, the membrane was washed once with TBST buffer (100 mM Tris-HCl pH 7.4, 154 mM NaCl, and 0.1% Tween 20) and then blocked with 5% goat or donkey serum in TBST for at least 1 h at room temperature. Three TBST wash steps were performed before the membrane was incubated overnight at 4℃ with rabbit polyclonal anti-α1-GlyR antibody (pAb α1, 1:1000, Chemicon), rat monoclonal anti-HA antibody (clone 3F10, 1:1000, Roche Applied Science, Mannheim, Germany) or rabbit polyclonal anti-α-tubulin antibody (1:1000, Cell Signaling Technology). The secondary horseradish peroxidase (HRP)-conjugated antibodies (1:10,000, Jackson ImmunoResearch Laboratories, West Grove, PA) were applied after four wash steps in TBST and incubated for 90 min at room temperature. After three final wash steps in TBST, signal detection was performed using Immun-Star^{TM} WesternC^{TM} Chemiluminescence in combination with Molecular Imager ChemiDoc XRS System (Bio-Rad Laboratories).

Immunocytochemistry

For analysis of GL261-endogenous GlyR α1 protein, cells were fixed for 10 min at −20℃ with a mixture (95:5) of methanol and glacial acetic acid and then processed for immunocytochemistry with a rabbit polyclonal antibody (1:300, Abcam, Cambridge, MA, USA) or the well-characterized mouse mAb2b antibody (1:100, Synaptic Systems). For detection of the surface-accessible Myc tag, the mouse monoclonal 9E10 antibody (1:100, Sigma) was used. For this purpose, the 9E10 antibody was applied directly to the cell culture and incubated for 10 min at 37℃ in incubator, washed three times with culture medium, fixed as described previously (Meier and Grantyn, 2004; Kowalczyk et al., 2013) and then processed for immunocytochemistry using the rat monoclonal 3F10 antibody (1:200, Roche Applied Science, Mannheim, Germany). Ubiquitin immunoreactivity was assessed using a polyclonal antibody (UB N-19) made in goat (1:100, Santa Cruz Biotechnology, Heidelberg, Germany). Following three wash steps, affinity-purified secondary donkey antibodies coupled to carboxymethyl indocyanine (Cy5) or fluorescein isothiocyanate (FITC) were used. The secondary antibodies were purchased from Jackson ImmunoResearch Laboratories (West Grove, PA, USA).

Microscopy and live-cell imaging

Fluorescent signals were acquired using the laser-scanning confocal microscope DM TCS SP5 (Leica Microsystems). Fluorochromes were excited sequentially to minimize cross-talk between fluorescent signals. Fluorescence was acquired using a HCX PL APO 40× UV oil objective (Leica Microsystems). Images were acquired using LCS software (Leica Microsystems) by multiple scanning and averaging of lines (eight times each). Live-cell imaging with confocal microscopy was performed likewise, except that multiple scanning was reduced to three frames per image. Cell nuclei and GlyR α3K were visualized using Hoechst 33342 (Invitrogen) and mCherry fluorescence, respectively. Optical sections were obtained along the *z*-axis using a 1-µm step size. Frames were acquired every minute. Movies were created using the software Imaris x64 7.6 (Bitplane Scientific Software, Zurich, Switzerland) and exported at a frame rate of 30 frames/s. For quantification of nuclear versus somatic GlyR distributions, integrated signal intensities were measured cell-wise within circular regions of interest (10 µm diameter) which were nucleus-centered and placed in the perinuclear cytoplasm as described previously (Winkelmann et al., 2014).

Statistics

Statistical analysis of tumor-cell-inoculated mice [Kaplan–Meier-survival-analysis, followed by log rank (Mantel–Cox), Breslow (generalised Wilcoxon) and Tarone-Ware test] was performed using the SPSS Statistics software (Predictive Analysis SoftWare 18, SPSS Inc., IBM Company Headquarters, Chicago, IL). One-way ANOVA analysis followed by post hoc Bonferroni test was used for statistical analysis of the subcellular GlyR distribution in GL261 cells. $P<0.05$ was considered significant.

Acknowledgements

We thank Anje Sporbert (Joint Intravital Microscopy and Imaging platform JIMI) for support and access to the SP5 confocal microscope, and Christina Eichhorn (SPSS & Statistik, IT, Max Delbrück Center for Molecular Medicine, Berlin, Germany) for performing statistical analyses with the SPSS software. We also thank Carola Bernert, Josephine Grosch, Anne Schäfer, Silke Dusatko and Andra Eisenmann at the Max Delbrück Center for Molecular Medicine for excellent technical assistance.

Competing interests

The authors declare no competing interests.

Author contributions

J.C.M. conceived the study. B.F., O.D.a D., and A.W. performed the majority of the experiments. M.Semtner and B.B. performed electrophysiological experiments. D.S.M., M.Synowitz and R.G. contributed to tumor inoculation. P.W. and M.F. helped with experiments related to analysis of gene expression. M.-P.J. provided ?the human stem-cell-like cell samples. J.C.M., B.F. and H.K. wrote the paper.

Funding

This study was supported by the Helmholtz Association [grant number VH-NG-246 to J.C.M.]; the Deutsche Forschungsgemeinschaft (DFG) [grant number SFB-TR3, project B5 to J.C.M.]; and the Bundesministerium für Bildung und Forschung (BMBF) [grant number ERA-Net NEURON II, project CIPRESS to J.C.M.].

Supplementary material

Supplementary material available online at
http://jcs.biologists.org/lookup/suppl/doi:10.1242/jcs.146662/-/DC1

References

Adewumi, O., Aflatoonian, B., Ahrlund-Richter, L., Amit, M., Andrews, P. W., Beighton, G., Bello, P. A., Benvenisty, N., Berry, L. S., Bevan, S. et al.; International Stem Cell Initiative (2007). Characterization of human embryonic stem cell lines by the International Stem Cell Initiative. *Nat. Biotechnol.* **25**, 803-816.

Bobek-Billewicz, B., Hebda, A., Stasik-Pres, G., Majchrzak, K., Zmuda, E. and Trojanowska, A. (2010). Measurement of glycine in a brain and brain tumors by means of 1H MRS. *Folia Neuropathol.* **48**, 190-199.

Breitinger, H. G. and Becker, C. M. (2002). The inhibitory glycine receptor-simple views of a complicated channel. *ChemBioChem* **3**, 1042-1052.

Büttner, C., Sadtler, S., Leyendecker, A., Laube, B., Griffon, N., Betz, H. and Schmalzing, G. (2001). Ubiquitination precedes internalization and proteolytic cleavage of plasma membrane-bound glycine receptors. *J. Biol. Chem.* **276**, 42978-42985.

Combet, C., Blanchet, C., Geourjon, C. and Deléage, G. (2000). NPS@: network protein sequence analysis. *Trends Biochem. Sci.* **25**, 147-150.

Del Pino, I., Koch, D., Schemm, R., Qualmann, B., Betz, H. and Paarmann, I. F. (2014). Proteomic analysis of glycine receptor β subunit (GlyRβ)-interacting proteins: evidence for syndapin I regulating synaptic glycine receptors. *J. Biol. Chem.* **289**, 11396-11409.

den Eynden, J. V., Ali, S. S., Horwood, N., Carmans, S., Brône, B., Hellings, N., Steels, P., Harvey, R. J. and Rigo, J. M. (2009). Glycine and glycine receptor signalling in non-neuronal cells. *Front Mol. Neurosci.* **2**, 9.

Eichler, S. A., Kirischuk, S., Jüttner, R., Schaefermeier, P. K., Legendre, P., Lehmann, T. N., Gloveli, T., Grantyn, R. and Meier, J. C. (2008). Glycinergic tonic inhibition of hippocampal neurons with depolarizing GABAergic transmission elicits histopathological signs of temporal lobe epilepsy. *J. Cell. Mol. Med.* **12**, 2848-2866.

Eichler, S. A., Förstera, B., Smolinsky, B., Jüttner, R., Lehmann, T. N., Fähling, M., Schwarz, G., Legendre, P. and Meier, J. C. (2009). Splice-specific roles of glycine receptor α3 in the hippocampus. *Eur. J. Neurosci.* **30**, 1077-1091.

Galan-Moya, E. M., Le Guelte, A., Lima Fernandes, E., Thirant, C., Dwyer, J., Bidere, N., Couraud, P. O., Scott, M. G., Junier, M. P., Chneiweiss, H. et al. (2011). Secreted factors from brain endothelial cells maintain glioblastoma stem-like cell expansion through the mTOR pathway. *EMBO Rep.* **12**, 470-476.

Glass, R., Synowitz, M., Kronenberg, G., Walzlein, J. H., Markovic, D. S., Wang, L. P., Gast, D., Kiwit, J., Kempermann, G. and Kettenmann, H. (2005). Glioblastoma-induced attraction of endogenous neural precursor cells is associated with improved survival. *J. Neurosci.* **25**, 2637-2646.

Grudzinska, J., Schemm, R., Haeger, S., Nicke, A., Schmalzing, G., Betz, H. and Laube, B. (2005). The beta subunit determines the ligand binding properties of synaptic glycine receptors. *Neuron* **45**, 727-739.

Harvey, R. J., Schmieden, V., Von Holst, A., Laube, B., Rohrer, H. and Betz, H. (2000). Glycine receptors containing the alpha4 subunit in the embryonic sympathetic nervous system, spinal cord and male genital ridge. *Eur. J. Neurosci.* **12**, 994-1001.

Hollmén, M., Liu, P., Kurppa, K., Wildiers, H., Reinvall, I., Vandorpe, T., Smeets, A., Deraedt, K., Vahlberg, T., Joensuu, H. et al. (2012). Proteolytic processing of ErbB4 in breast cancer. *PLoS ONE* **7**, e39413.

Huang, R., He, S., Chen, Z., Dillon, G. H. and Leidenheimer, N. J. (2007). Mechanisms of homomeric alpha1 glycine receptor endocytosis. *Biochemistry* **46**, 11484-11493.
Jain, M., Nilsson, R., Sharma, S., Madhusudhan, N., Kitami, T., Souza, A. L., Kafri, R., Kirschner, M. W., Clish, C. B. and Mootha, V. K. (2012). Metabolite profiling identifies a key role for glycine in rapid cancer cell proliferation. *Science* **336**, 1040-1044.
Jiang, T., Olson, E. S., Nguyen, Q. T., Roy, M., Jennings, P. A. and Tsien, R. Y. (2004). Tumor imaging by means of proteolytic activation of cell-penetrating peptides. *Proc. Natl. Acad. Sci. USA* **101**, 17867-17872.
Kowalczyk, S., Winkelmann, A., Smolinsky, B., Förstera, B., Neundorf, I., Schwarz, G. and Meier, J. C. (2013). Direct binding of $GABA_A$ receptor β2 and β3 subunits to gephyrin. *Eur. J. Neurosci*. **37**, 544-554.
Kuhse, J., Kuryatov, A., Maulet, Y., Malosio, M. L., Schmieden, V. and Betz, H. (1991). Alternative splicing generates two isoforms of the alpha 2 subunit of the inhibitory glycine receptor. *FEBS Lett.* **283**, 73-77.
Labrakakis, C., Patt, S., Hartmann, J. and Kettenmann, H. (1998). Functional GABA(A) receptors on human glioma cells. *Eur. J. Neurosci.* **10**, 231-238.
Laks, D. R., Masterman-Smith, M., Visnyei, K., Angenieux, B., Orozco, N. M., Foran, I., Yong, W. H., Vinters, H. V., Liau, L. M., Lazareff, J. A. et al. (2009). Neurosphere formation is an independent predictor of clinical outcome in malignant glioma. *Stem Cells* **27**, 980-987.
Legendre, P., Förstera, B., Jüttner, R. and Meier, J. C. (2009). Glycine receptors caught between genome and proteome – Functional implications of RNA editing and splicing. *Front. Mol. Neurosci.* **2**, 23.
Malosio, M. L., Grenningloh, G., Kuhse, J., Schmieden, V., Schmitt, B., Prior, P. and Betz, H. (1991). Alternative splicing generates two variants of the alpha 1 subunit of the inhibitory glycine receptor. *J. Biol. Chem.* **266**, 2048-2053.
Meier, J. and Grantyn, R. (2004). Preferential accumulation of GABA(A) receptor γ2L, not γ2S, cytoplasmic loops at rat spinal cord inhibitory synapses. *J. Physiol*. **559**, 355-365.
Meier, J., Vannier, C., Sergé, A., Triller, A. and Choquet, D. (2001). Fast and reversible trapping of surface glycine receptors by gephyrin. *Nat. Neurosci.* **4**, 253-260.
Meier, J., Jüttner, R., Kirischuk, S. and Grantyn, R. (2002). Synaptic anchoring of glycine receptors in developing collicular neurons under control of metabotropic glutamate receptor activity. *Mol. Cell. Neurosci.* **21**, 324-340.
Melzer, N., Villmann, C., Becker, K., Harvey, K., Harvey, R. J., Vogel, N., Kluck, C. J., Kneussel, M. and Becker, C. M. (2010). Multifunctional basic motif in the glycine receptor intracellular domain induces subunit-specific sorting. *J. Biol. Chem*. **285**, 3730-3739.
Meyer, G., Kirsch, J., Betz, H. and Langosch, D. (1995). Identification of a gephyrin binding motif on the glycine receptor beta subunit. *Neuron* **15**, 563-572.
Nanba, D., Mammoto, A., Hashimoto, K. and Higashiyama, S. (2003). Proteolytic release of the carboxy-terminal fragment of proHB-EGF causes nuclear export of PLZF. *J. Cell Biol.* **163**, 489-502.
Nikolic, Z., Laube, B., Weber, R. G., Lichter, P., Kioschis, P., Poustka, A., Mülhardt, C. and Becker, C. M. (1998). The human glycine receptor subunit alpha3. Glra3 gene structure, chromosomal localization, and functional characterization of alternative transcripts. *J. Biol. Chem.* **273**, 19708-19714.
Notelaers, K., Smisdom, N., Rocha, S., Janssen, D., Meier, J. C., Rigo, J. M., Hofkens, J. and Ameloot, M. (2012). Ensemble and single particle fluorimetric techniques in concerted action to study the diffusion and aggregation of the glycine receptor α3 isoforms in the cell plasma membrane. *Biochim. Biophys. Acta* **1818**, 3131-3140.
Silvestre, D. C., Pineda, J. R., Hoffschir, F., Studler, J. M., Mouthon, M. A., Pflumio, F., Junier, M. P., Chneiweiss, H. and Boussin, F. D. (2011). Alternative lengthening of telomeres in human glioma stem cells. *Stem Cells* **29**, 440-451.
Simon, J., Wakimoto, H., Fujita, N., Lalande, M. and Barnard, E. A. (2004). Analysis of the set of GABA(A) receptor genes in the human genome. *J. Biol. Chem.* **279**, 41422-41435.
Tasneem, A., Iyer, L. M., Jakobsson, E. and Aravind, L. (2004). Identification of the prokaryotic ligand-gated ion channels and their implications for the mechanisms and origins of animal Cys-loop ion channels. *Genome Biol.* **6**, R4.
Thirant, C., Bessette, B., Varlet, P., Puget, S., Cadusseau, J., Tavares, S. R., Studler, J. M., Silvestre, D. C., Susini, A., Villa, C. et al. (2011). Clinical relevance of tumor cells with stem-like properties in pediatric brain tumors. *PLoS ONE* **6**, e16375.
Walzlein, J. H., Synowitz, M., Engels, B., Markovic, D. S., Gabrusiewicz, K., Nikolaev, E., Yoshikawa, K., Kaminska, B., Kempermann, G., Uckert, W. et al. (2008). The antitumorigenic response of neural precursors depends on subventricular proliferation and age. *Stem Cells* **26**, 2945-2954.
Winkelmann, A., Maggio, N., Eller, J., Caliskan, G., Semtner, M., Häussler, U., Jüttner, R., Dugladze, T., Smolinsky, B., Kowalczyk, S. et al. (2014). Changes in neural network homeostasis trigger neuropsychiatric symptoms. *J. Clin. Invest.* **124**, 696-711.
Zuleger, N., Kerr, A. R. and Schirmer, E. C. (2012). Many mechanisms, one entrance: membrane protein translocation into the nucleus. *Cell. Mol. Life Sci.* **69**, 2205-2216.

Journal of Cell Science

Supplemental information

Intracellular glycine receptor function facilitates glioma formation in vivo

Benjamin Förstera[1*], Omar Dildar a Dzaye[2*], Aline Winkelmann[1,3], Marcus Semtner[1], Bruno Benedetti[4], Darko S. Markovic[5], Michael Synowitz[6], Peter Wend[7], Michael Fähling[8], Marie-Pierre Junier[9], Rainer Glass[10], Helmut Kettenmann[2] and Jochen C. Meier[1]

[1] RNA editing and Hyperexcitability Disorders Helmholtz Group, Max Delbrück Center for Molecular Medicine, 13092 Berlin, Germany
[2] Cellular Neuroscience, Max Delbrück Center for Molecular Medicine, 13092 Berlin, Germany
[3] FU-Berlin, Fachbereich Biologie, Chemie, Pharmazie, Takustr. 3, 14195 Berlin
[4] Department for Physiology, Innsbruck Medical University, 6020 Innsbruck, Austria
[5] Department for Neurosurgery, Helios Clinical Center, 13125 Berlin, Germany
[6] Department for Neurosurgery, Charité Universitätsmedizin Berlin, 13353 Berlin, Germany
[7] David Geffen School of Medicine at UCLA, UCLA Jonsson Comprehensive Cancer Center, 10833 LeConte Ave., CHS 27-139, Los Angeles, CA. 90095, USA
[8] Institut für Vegetative Physiologie, Charité Universitätsmedizin Berlin, 10115 Berlin, Germany
[9] INSERM U894, Psychiatry and Neuroscience Center, Glial Plasticity Team, Paris, France
[10] Neurosurgical Research, University Clinics Munich, 81377 München, Germany
[*] Equal contribution

Correspondence:
Dr. Jochen C. Meier
Max Delbrück Center for Molecular Medicine
Robert-Rössle-Straße 10, 13092 Berlin
Germany
Phone: +49-(0)30-94063062
Email: jochen.meier@mdc-berlin.de

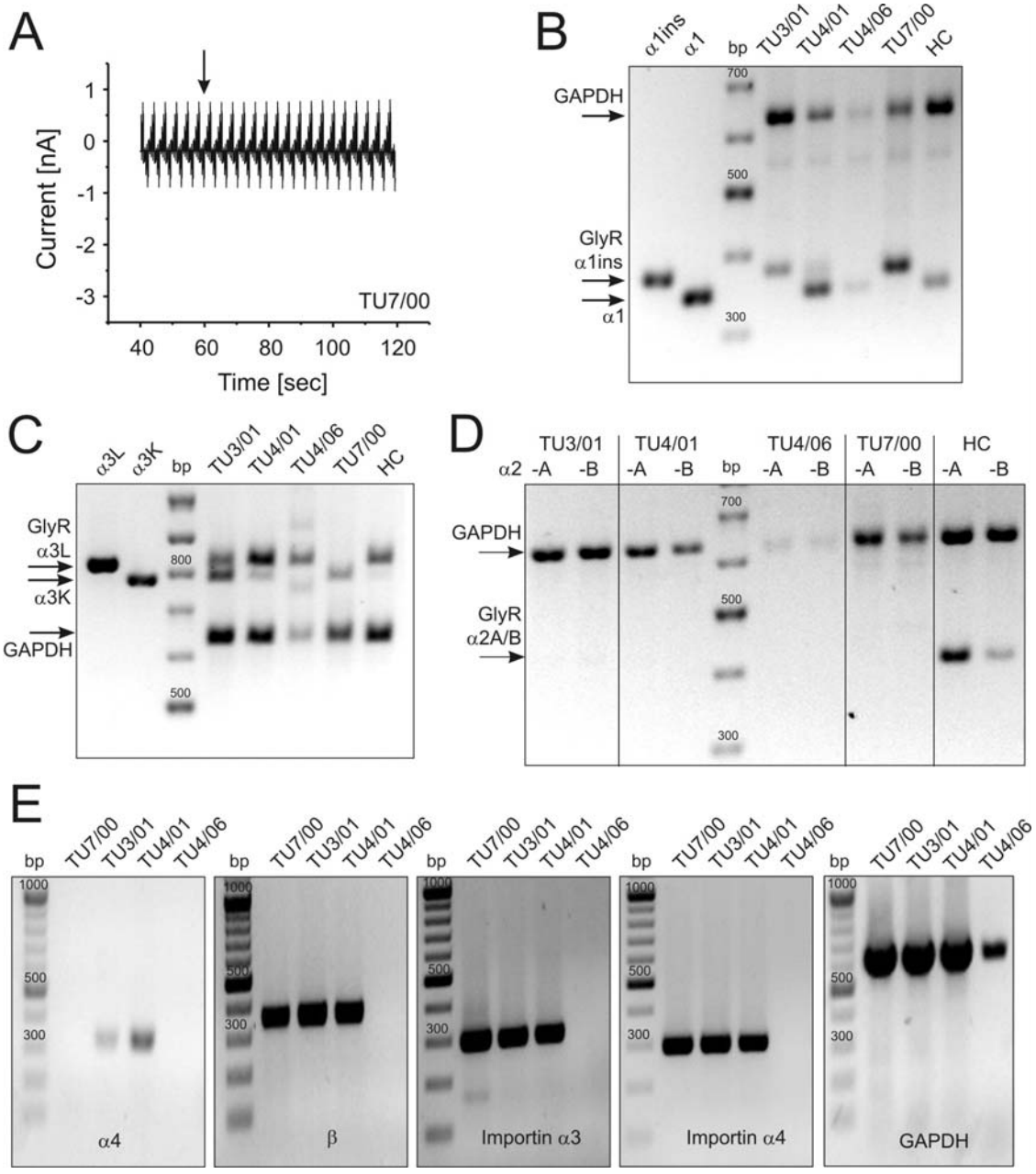

Suppl. Fig. 1: (**A**) Cultured human brain tumor cells do not respond to application of glycine. Representative current profile upon voltage ramps during a recording of human glioma cells (TU7/00). The arrow marks onset of glycine application (500 µM). Note that glycine failed to induce Cl^- currents in cultured human glioma cells. (**B-E**) RT-PCR analysis of GlyR and importin expression in cell culture of glioblastoma multiforme TU7/00, TU3/01, TU4/06 (WHO grade IV), and primitive neuroectodermal tumor (TU4/01). Cells were processed for RT-PCR with oligonucleotides specific to GlyR α1 (**B**), α3 (**C**), α2 (**D**) as well as α4, β, and importin α3 and α4 (**E**). For positive control purpose, human post-mortem hippocampus (HC) and GlyR cDNA clones were included (**B-D**). To verify presence of mRNA, cDNA coding for the house keeping gene *GAPDH* was co-amplified in parallel in all cases.

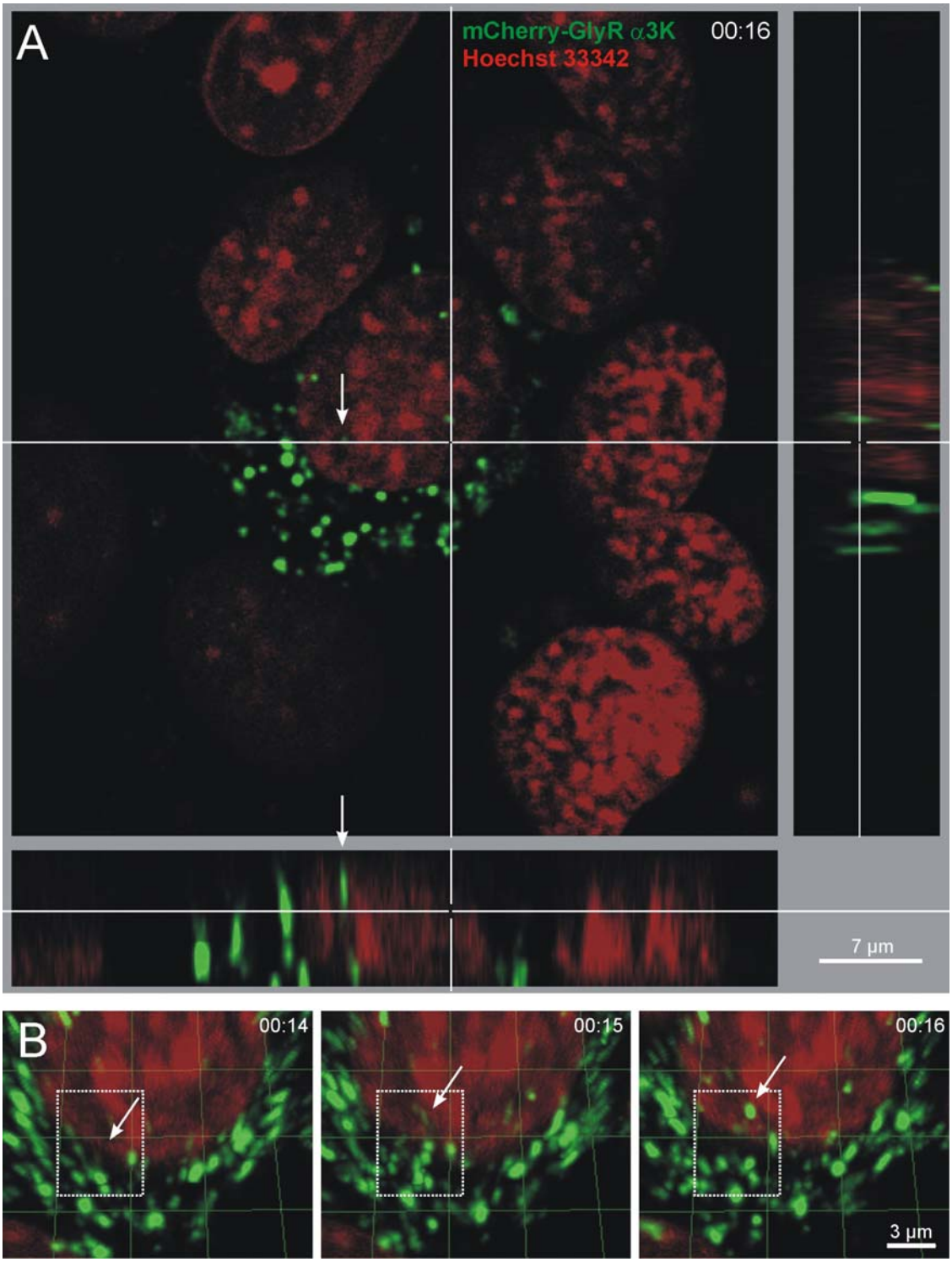

Suppl. Fig. 2: (**A**) The image shows a confocal section (1 µm thick) of the mCherry-GlyR α3K-expressing GL261 cell shown in Figure 6. White lines indicate positions of Z-sections (0.408 µm width) along X and Y axes shown below (X) and right hand (Y), respectively, to the image. The arrow points to an intranuclear mCherry-GlyR α3K cluster (green). Quantitative data are presented in Suppl. Table 3. (**B**) Tilted view of Z-stack projections showing mCherry-GlyR α3K dynamics within a 2 min recording

interval (00:14-00:16). The dashed box delineates a region where rapid translocation (arrows) of mCherry-GlyR α3K (green) to the nuclear compartment of the GL261 cell (Hoechst 33342, red) occurred (see also Fig. 6B, arrows).

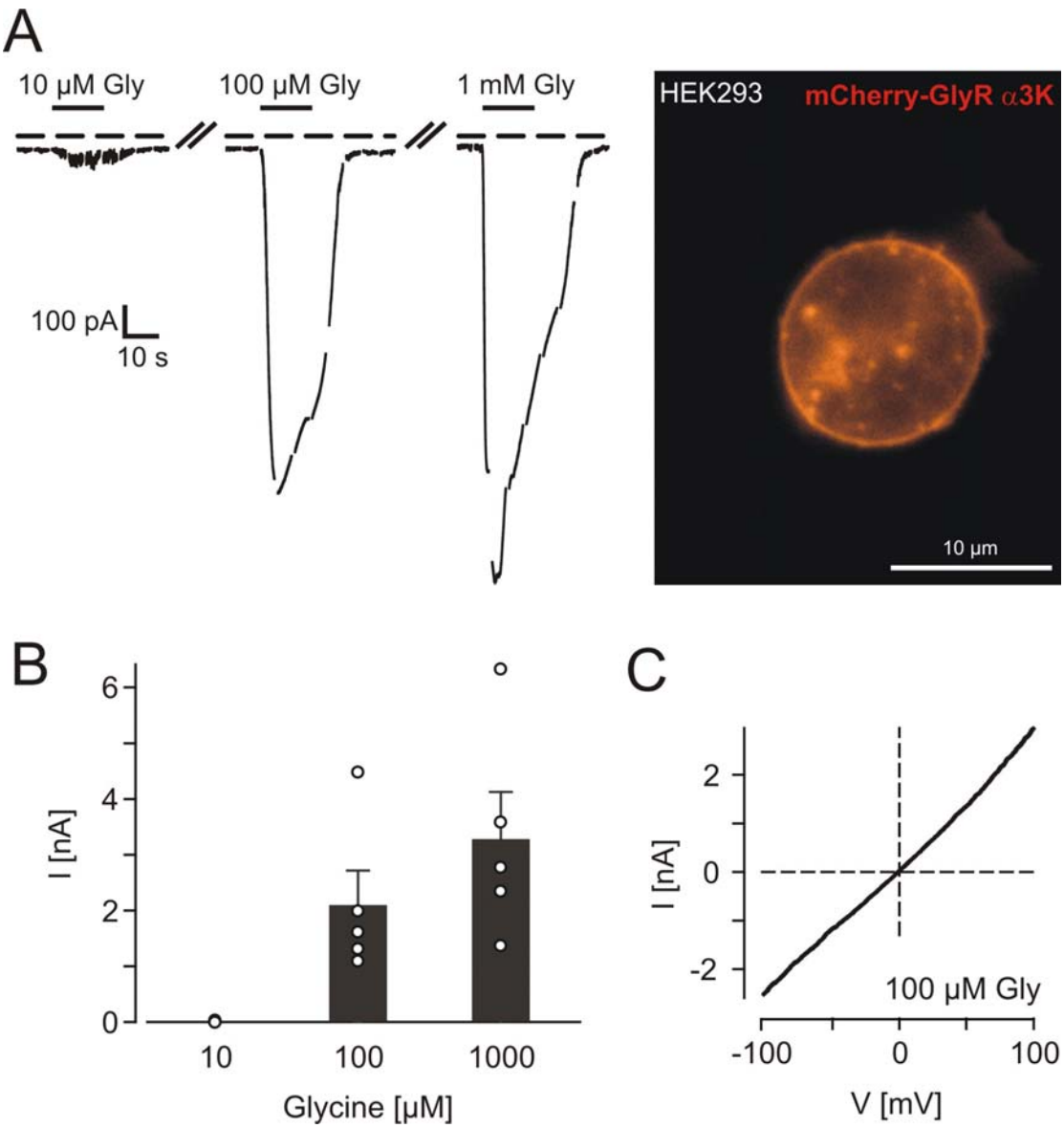

Suppl. Fig. 3: Electrophysiological and optical analyses of mCherry-GlyR α3K-expressing HEK293 cells. (**A**) The example traces show current responses to application of indicated glycine concentrations (Cl^- driving force: -50 mV). The fluorescence profile of a patched cell is shown right-hand. (**B**) Quantification of the current amplitudes obtained in response to application of the different glycine concentrations. (**C**) Current-voltage relationship obtained using 100 µM glycine show that mCherry-GlyR α3K formed Cl^--permeable neurotransmitter receptors at the HEK293 cell surface. Clearly, mCherry-GlyR α3K accessed the cell surface of HEK293 cells and generated transmembrane Cl^- currents.

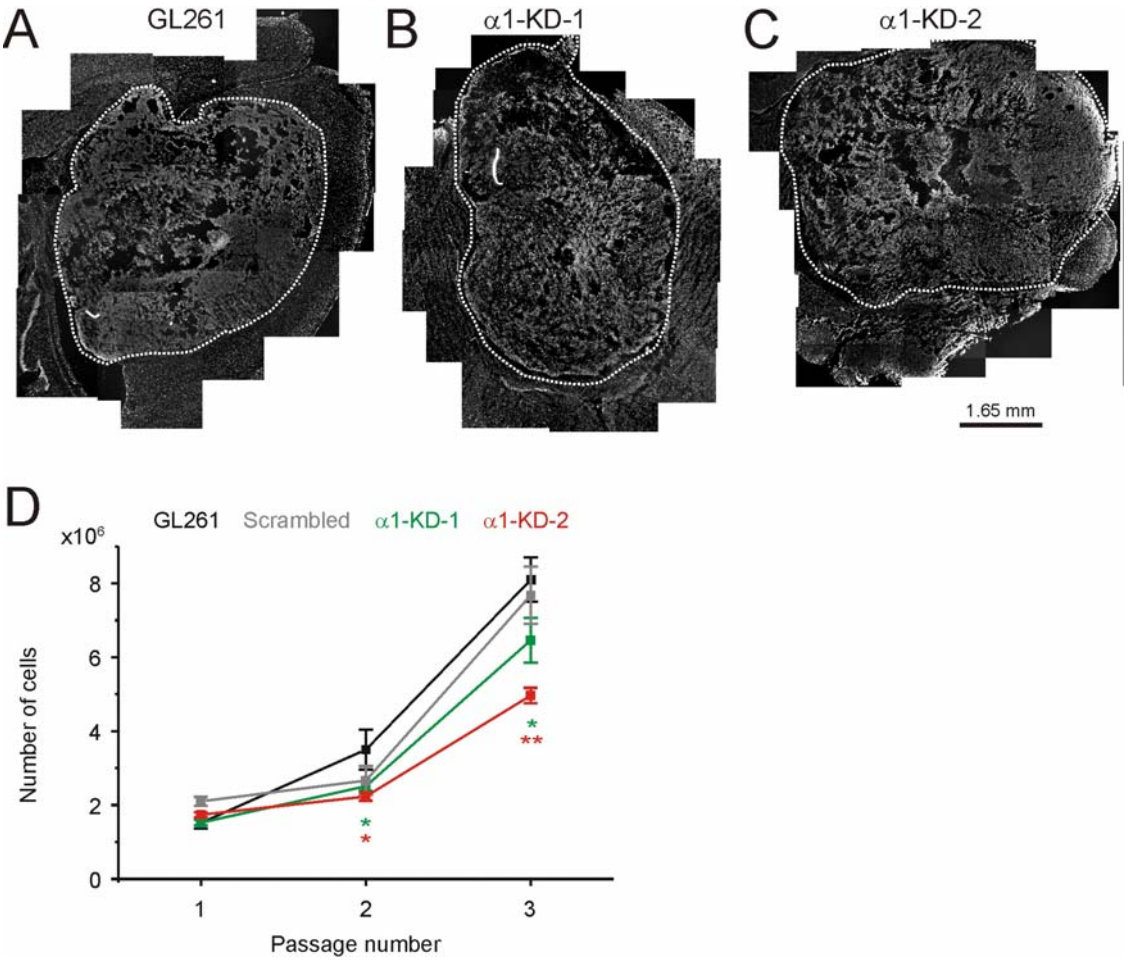

Suppl. Fig. 4: Post-mortem analysis of DAPI stained brain sections show similarly sized brain tumors formed by GL261 (**A**), α1-KD-1 (**B**), or α1-KD-2 (**C**) cells. (**D**) Analysis of cell proliferation. GL261, scrambled-shRNA-expressing GL261, α1-KD-1, and α1-KD-2 cells were seeded in 10 cm culture dishes ($1x10^6$ cells each). At each sub-culturing passage every three days cell numbers were determined using a Neubauer counting chamber. Three consecutive passages revealed an inhibiting effect of GlyR α1 knockdown on GL261 cell proliferation. Significant differences between GL261 and α1-KD-1/2 cells are indicated as *: $P < 0.05$, **: $P < 0.01$ (one-way Anova, post-hoc Bonferroni).

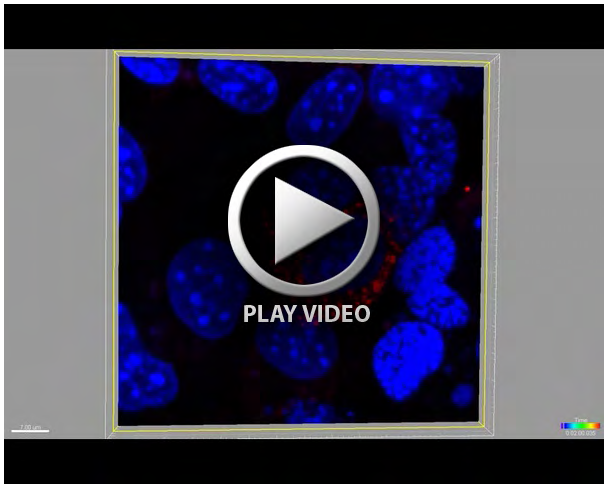

Movie 1. The movie (duration of 3 seconds, sampled at 30 frames per second) shows projected z-stacks of mCherry–GlyR-α3K and Hoechst 33342 fluorescent signals (red and blue, respectively) acquired during a 90-min imaging interval of a transfected GL261 cell. Each frame represents the projection of 10 z-sections acquired with 1-µm step size (z-stack).

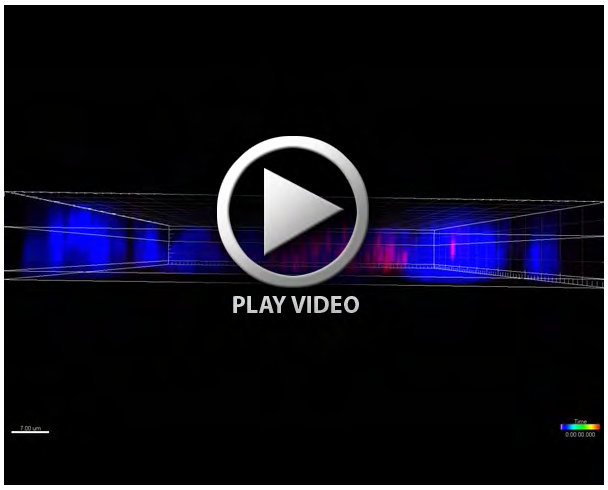

Movie 2. The movie (duration of 3 seconds, sampled at 30 frames per second) shows a side view of the transfected GL261 cell shown in Suppl. Movie 1.

Movie 3. The movie (duration of 3 seconds, sampled at 30 frames per second) shows projected z-stacks of mCherry–GlyR-α3K and Hoechst 33342 fluorescent signals (red and blue, respectively) of another transfected GL261 cell. Each frame represents the projection of 10 z-sections acquired with 1-µm step size (z-stack).

Suppl. Table 1:
Overview of resected tumor tissue samples in the brain cancer tissue array used for quantitative real-time PCR

Color code for GlyR-positive samples: GLRA1 | GLRA3 | GLRA1 + GLRA3

SKU	Well	Well position	Gender	Age	Tissue of (Origin/Finding)	Appearance	Sample diagnosis from pathology verification	Case diagnosis from Donor Institution pathology report	Tumor Grade	Pathology Verification Notes
HBRT102/302/502	1	C1	Female	55	Brain / Brain	Normal	Within normal limits	Within normal limits		Non Tumor Structures: 80% Gray matter, 20% White matter
HBRT102/302/502	2	C2	Male	60	Brain / Brain	Normal	Within normal limits	Within normal limits		Non Tumor Structures: 40% Gray matter, 60% White matter
HBRT102/302/502	3	C3	Female	56	Brain / Brain	Tumor	Meningioma, fibroblastic	Meningioma, fibroblastic	WHO Grade I	Inflammatory cells present in stroma
HBRT102/302/502	4	C4	Female	51	Brain / Brain	Tumor	Meningioma, fibroblastic	Meningioma, fibroblastic	WHO Grade I	
HBRT102/302/502	5	C5	Male	71	Brain / Brain	Tumor	Meningioma	Meningioma	WHO Grade I	
HBRT102/302/502	6	C6	Female	56	Brain / Brain	Tumor	Meningioma, meningothelial	Meningioma, benign	WHO Grade I	
HBRT102/302/502	7	C7	Female	41	Brain / Brain	Tumor	Meningioma, secretory	Meningioma, secretory	WHO Grade I	
HBRT102/302/502	8	C8	Female	42	Brain / Brain	Tumor	Meningioma	Meningioma	WHO Grade I	Tumor Stroma (Hypo/Acellular): calcifications
HBRT102/302/502	9	C9	Female	73	Brain / Brain	Tumor	Meningioma	Meningioma	WHO Grade I	
HBRT102/302/502	10	C10	Female	64	Meninges / Brain	Tumor	Meningioma, meningothelial	Meningioma, meningothelial	WHO Grade I	
HBRT102/302/502	11	C11	Male	39	Brain / Brain	Tumor	Meningioma, fibroblastic	Meningioma, fibroblastic	WHO Grade I	
HBRT102/302/502	12	C12	Male	43	Brain / Brain	Tumor	Meningioma, fibroblastic	Meningioma, fibroblastic	WHO Grade I	
HBRT102/302/502	13	D1	Female	27	Brain / Brain	Tumor	Astrocytoma	Astrocytoma	WHO Grade I	Tumor: Pilocytic type
HBRT102/302/502	14	D2	Female	83	Meninges / Brain	Tumor	Meningioma	Meningioma	WHO Grade I	
HBRT102/302/502	15	D3	Male	68	Meninges / Brain	Tumor	Meningioma	Meningioma	WHO Grade I	
HBRT102/302/502	16	D4	Female	45	Meninges / Brain	Tumor	Meningioma	Meningioma	WHO Grade I	
HBRT102/302/502	17	D5	Female	61	Meninges / Brain	Tumor	Meningioma	Meningioma	WHO Grade I	Cautery artifact present
HBRT102/302/502	18	D6	Male	44	Brain / Brain	Tumor	Meningioma	Meningioma	WHO Grade I	
HBRT102/302/502	19	D7	Male	61	Brain / Brain	Tumor	Meningioma, angiomatous	Meningioma	WHO Grade I	
HBRT102/302/502	20	D8	Female	54	Meninges / Brain	Tumor	Meningioma	Meningioma	WHO Grade I	Tumor Stroma (Cellular): Foamy histiocytes
HBRT102/302/502	21	D9	Female	63	Meninges / Brain	Tumor	Meningioma, meningothelial	Meningioma, meningothelial	WHO Grade II	
HBRT102/302/502	22	D10	Female	50	Brain / Brain	Tumor	Astrocytoma, fibrillary	Astrocytoma, fibrillary	WHO Grade II	Sample contains 50% normal grey & white matter in normal component
HBRT102/302/502	23	D11	Male	67	Brain / Brain	Tumor	Meningioma, atypical	Meningioma, atypical	WHO Grade II	
HBRT102/302/502	24	D12	Male	45	Brain / Brain	Lesion	Gliosis	Oligodendroglioma	WHO Grade II	lesion: 95% glial cells, 5% vessels
HBRT102/302/502	25	E1	Female	37	Brain / Brain	Tumor	Oligoastrocytoma	Oligoastrocytoma	WHO Grade II	
HBRT102/302/502	26	E2	Male	26	Brain / Brain	Tumor	Astrocytoma	Astrocytoma	WHO Grade II	
HBRT102/302/502	27	E3	Female	56	Meninges / Brain	Tumor	Meningioma, meningothelial	Meningioma, meningothelial	WHO Grade II	Cautery artifact noted
HBRT102/302/502	28	E4	Female	53	Brain / Brain	Tumor	Astrocytoma	Astrocytoma	WHO Grade II	
HBRT102/302/502	29	E5	Male	73	Brain / Brain	Tumor	Meningioma, atypical	Meningioma, clear cell	WHO Grade II	Tumor: clear cell type; Tumor Stroma (Hypo/Acellular): hyalinization
HBRT102/302/502	30	E6	Female	48	Brain / Brain	Tumor	Meningioma, atypical	Meningioma, atypical	WHO Grade II	
HBRT102/302/502	31	E7	Male	33	Brain / Brain	Tumor	Oligodendroglioma	Oligodendroglioma	WHO Grade II	
HBRT102/302/502	32	E8	Male	36	Brain / Brain	Tumor	Astrocytoma, anaplastic	Astrocytoma, anaplastic	WHO Grade III	
HBRT102/302/502	33	E9	Male	39	Brain / Brain	Tumor	Astrocytoma, anaplastic	Astrocytoma, anaplastic	WHO Grade III	
HBRT102/302/502	34	E10	Male	30	Brain / Brain	Tumor	Astrocytoma	Astrocytoma, anaplastic	WHO Grade III	
HBRT102/302/502	35	E11	Male	46	Brain / Brain	Tumor	Oligodendroglioma, anaplastic	Oligodendroglioma, anaplastic	WHO Grade III	
HBRT102/302/502	36	E12	Female	41	Brain / Brain	Tumor	Oligodendroglioma, anaplastic	Oligodendroglioma, anaplastic	WHO Grade III	
HBRT102/302/502	37	F1	Female	49	Brain / Brain	Tumor	Ependymoma of brain, anaplastic	Ependymoma of brain, anaplastic	WHO Grade III	
HBRT102/302/502	38	F2	Male	41	Brain / Brain	Tumor	Oligoastrocytoma, anaplastic	Oligoastrocytoma, anaplastic	WHO Grade III	Anaplastic oligoastrocytoma
HBRT102/302/502	39	F3	Female	51	Brain / Brain	Tumor	Oligodendroglioma, anaplastic	Oligodendroglioma, anaplastic	WHO Grade III	
HBRT102/302/502	40	F4	Female	32	Brain / Brain	Tumor	Astrocytoma, anaplastic	Astrocytoma, anaplastic	WHO Grade III	
HBRT102/302/502	41	F5	Female	44	Brain / Brain	Tumor	Oligodendroglioma, anaplastic	Oligodendroglioma, anaplastic	WHO Grade III	
HBRT102/302/502	42	F6	Male	66	Brain / Brain	Tumor	Glioblastoma multiforme	Glioblastoma multiforme	WHO Grade IV	
HBRT102/302/502	43	F7	Male	47	Brain / Brain	Tumor	Glioblastoma multiforme	Glioblastoma multiforme	WHO Grade IV	
HBRT102/302/502	44	F8	Female	71	Brain / Brain	Tumor	Meningioma, microcystic	Meningioma, microcystic	Not Reported	
HBRT102/302/502	45	F9	Female	40	Brain / Brain	Tumor	Meningioma, meningothelial	Meningioma, meningothelial	Not Reported	
HBRT102/302/502	46	F10	Male	63	Brain / Brain	Tumor	Hemangiopericytoma of brain	Hemangiopericytoma of brain	Not Reported	Tumor Stroma (Hypo/Acellular): Fibrosis
HBRT102/302/502	47	F11	Female	46	Brain / Brain	Tumor	Meningioma	Meningioma	Not Reported	
HBRT102/302/502	48	F12	Female	66	Brain / Brain	Tumor	Hemangiopericytoma of brain	Hemangiopericytoma of brain	Not Reported	

Suppl. Table 2: Overview of GlyR expression in human stem-like tumor cells.

Stem-like cells derived from	Internal reference	Passage number	GlyR α1	GlyR α1ins	GlyR α3K	GlyR α3L
Adult glioma (III)	OB1	P36			+	
Adult GBM (IV)	TG1N	P23		+	+	**(+)**
Adult GBM (IV)	TG10	P7		+	+	
Adult GBM (IV)	TG16	P14				+
Adult GBM (IV)	TG29	P15			+	**(+)**
Adult GBM (IV)	TG30	P10		+	+	
Pediatric glioma (II)	TP54	P15			+	
Pediatric glioma (III)	TP59	P28			+	**(+)**
Pediatric glioma (III)	TP80	P26	+		+	
Pediatric glioma (III)	TP83	P26			+	**(+)**
Pediatric glioma (III)	TP84	P14	+			+

PCR oligonucleotides span alternatively spliced regions and identify GlyR RNA splice variants as aforementioned (Suppl. Fig. 1). Tumor grading is indicated in brackets. GlyR-expressing samples are marked with '+'. Samples with stronger relative expression of α3K compared to α3L are marked with '(+)'. GBM = glioblastoma multiforme.

Suppl. Table 3: Summary of subcellular GlyR distribution in GL261 cells

	Grey level ratio (nucleus/cytoplasm)
α1 (cell endogenous)	1.09 ± 0.07 (n=46) ***
myc-α1ins-NLS-HA	0.87 ± 0.03 (n=48)
myc-α1ins-NLS-ΔLL-α2-HA	0.75 ± 0.03 (n=54)
myc-α1ins -ΔLL-ΔNLS -α2-HA	0.17 ± 0.01 (n=75) ***
myc-α2B-HA	0.15 ± 0.02 (n=44) ***
mCherry-α3K	0.80 ± 0.03 (n=26)

Summary of the cell-wise quantification of integrated fluorescence intensities measured within circular (10 µm diameter) regions of interest which were nucleus-centered or positioned in the perinuclear cytoplasmic compartment of GL261 cells. Asterisks denote significant differences in comparison to GL261 cells with GlyR myc-α1ins-NLS-HA expression (***: $P < 0.001$).

Suppl. Table 4: Quantitative real-time PCR on GL261, α1-KD-1 and α1-KD-2 in mouse stem cell pluripotency array. Results are listed according to their position in the array. Threshold cycles (Ct) are shown as detected. Relative mRNA levels in knock-down samples compared to GL261 control are indicated in percent. Assuming a two-fold increase of PCR product per cycle, relative mRNA levels were calculated as 2^{-n}, with *n* being the difference between Ct after normalizing Ct to *HPRT1* in GL261, the endogenous control gene with comparable mRNA levels in the three cell samples (well A3, bold). When Ct were above 40 (cut-off), probes were labeled 'nd' (gray). Relative mRNA was not calculated if Ct were above 40 in GL261 and knock-down cell samples. If one Ct was above 40 while mRNA expression was detected in the other cell sample, it was assigned the value of 40 to estimate relative mRNA levels in samples with detectable mRNA expression.

Well	Gene	Assay	Cell type marker	Threshold cycle (Ct)			*Hprt*-normalzed mRNA relative to GL261 [%]	
				GL261	α1-KD-1	α1-KD-2	α1-KD-1	α1-KD-2
A1	*18S*	18S-Hs99999901_s1	Endogenous Control	14,93	14,15	14,27	172	144
A2	*Gapdh*	Gapdh-Mm99999915_g1	Endogenous Control	17,04	17,4	17,68	78	57
A3	*Hprt1*	Hprt1-Mm00446968_m1	Endogenous Control	**23,84**	**23,85**	**23,62**	100	100
A4	*Gusb*	Gusb-Mm00446953_m1	Endogenous Control	24,23	24,09	24,62	111	65
A5	*Actc1*	Actc1-Mm01333821_m1	Cardiac Muscle	38,01	36,99	38,47	205	57
A6	*Afp*	Afp-Mm00431715_m1	Visceral Endoderm	nd	nd	nd	nd	nd
A7	*Bxdc2*	Bxdc2-Mm00503229_m1	Stem Cell	22,86	23,1	23,91	85	41
A8	*Cd34*	Cd34-Mm00519283_m1	Endothelial	nd	nd	nd	nd	nd
A9	*Cd9*	Cd9-Mm00514275_g1	Stem Cell	19,63	19,85	19,64	86	87
A10	*Cdh5*	Cdh5-Mm00486938_m1	Endothelial	39,57	35,98	nd	1217	57
A11	*Cdx2*	Cdx2-Mm00432449_m1	Trophoblast	nd	nd	nd	nd	nd
A12	*Col1a1*	Col1a1-Mm00801666_g1	Bone	21,9	21,22	24,12	161	18
B1	*Col2a1*	Col2a1-Mm00491889_m1	Cartilage	27,9	26,13	29,72	344	23
B2	*Commd3*	Commd3-Mm00521684_m1	Stem Cell	24,28	24,32	24,69	98	64
B3	*Crabp2*	Crabp2-Mm00801693_g1	Stem Cell	21,79	22,34	20,95	69	156
B4	*Ddx4*	Ddx4-Mm00802445_m1	Germ Cell	36,57	36,4	36,78	114	68
B5	*Des*	Des-Mm00802455_m1	Muscle	nd	nd	nd	nd	nd
B6	*Dnmt3b*	Dnmt3b-Mm01240113_m1	Stem Cell	29,28	29,75	30,76	73	29
B7	*Lefty1*	Lefty1-Mm00438615_m1	Stem Cell	38,55	38,62	nd	96	28
B8	*Eomes*	Eomes-Mm01351985_m1	Trophoblast	35,4	36,88	39,23	36	5
B9	*Fgf4*	Fgf4-Mm00438917_m1	Stem Cell	nd	39,27	nd	168	nd
B10	*Fgf5*	Fgf5-Mm00438919_m1	Stem Cell	nd	nd	nd	nd	nd
B11	*Flt1*	Flt1-Mm00438980_m1	Endothelial	28,82	30,96	29,5	23	52
B12	*Fn1*	Fn1-Mm01256744_m1	Parietal Endoderm	23,82	21,95	26,08	368	18
C1	*Foxa2*	Foxa2-Mm01976556_s1	Extraembryonic endoderm	nd	38,4	39,46	307	113
C2	*Foxd3*	Foxd3-Mm02384867_s1	Stem Cell	nd	nd	nd	nd	nd
C3	*Gabrb3*	Gabrb3-Mm00433473_m1	Stem Cell	nd	38,03	nd	396	nd
C4	*Gal*	Gal-Mm00439056_m1	Stem Cell	35,58	38,01	37,27	19	24
C5	*Gata4*	Gata4-Mm00484689_m1	Extraembryonic endoderm	35,68	36,71	35,53	49	88
C6	*Gata6*	Gata6-Mm00802636_m1	Stem Cell	28,66	30,64	28,7	26	81
C7	*Gbx2*	Gbx2-Mm00494578_m1	Stem Cell	nd	nd	nd	nd	nd
C8	*Gcg*	Gcg-Mm00801712_m1	Pancreas	37,18	35,7	36,64	282	115
C9	*Gcm1*	Gcm1-Mm00492310_m1	Trophoblast	39,32	38,92	nd	133	48
C10	*Gdf3*	Gdf3-Mm00433563_m1	Stem Cell	35,89	36,84	35,92	52	78
C11	*Gfap*	Gfap-Mm00546086_m1	Astrocytes	27,21	27,76	27,59	69	64
C12	*Grb7*	Grb7-Mm01306734_m1	Stem Cell	26,61	28,03	28,94	38	16
D1	*Hbb-b2*	Hbb-b2-Mm00731743_mH	Blood	nd	nd	nd	nd	nd
D2	*Hba-x*	Hba-x-Mm00439255_m1	Blood	38,8	38,4	nd	133	34
D3	*Mnx1*	Mnx1-Mm00658300_g1	Motorneurons & Pancreas	nd	nd	nd	nd	nd
D4	*Iapp*	Iapp-Mm00439403_m1	Pancreas	29,23	28,27	29,77	196	57
D5	*Ifitm1*	Ifitm1-Mm00850040_g1	Stem Cell	34,19	34,3	33,82	94	104
D6	*Ifitm2*	Ifitm2-Mm00850080_g1	Stem Cell	20,24	20,37	20,42	92	77

Well	Gene	Assay	Cell type marker	Threshold cycle (Ct)			*Hprt*-normalized mRNA relative to GL261 [%]	
				GL261	α1-KD-1	α1-KD-2	α1-KD-1	α1-KD-2
D7	*Il6st*	Il6st-Mm00439668_m1	Stem Cell	26,57	27	27,22	75	53
D8	*Igfbp2*	Igfbp2-Mm00492632_m1	Pancreas	nd	nd	nd	nd	nd
D9	*Ins2*	Ins2-Mm00731595_gH	Pancreas	38,15	nd	38,47	28	62
D10	*Pdx1*	Pdx1-Mm00435565_m1	Pancreas	nd	nd	nd	nd	nd
D11	*Isl1*	Isl1-Mm00627860_m1	V3 Interneurons	32,57	35,04	32,51	18	85
D12	*Kit*	Kit-Mm00445212_m1	Stem Cell	31,55	32,57	35,68	50	5
E1	*Krt1*	Krt1-Mm00492992_g1	Trophoblast	nd	38,49	38,04	288	304
E2	*Lama1*	Lama1-Mm00439445_m1	Parietal Endoderm	nd	nd	nd	nd	nd
E3	*Lamb1-1*	Lamb1-1-Mm00801853_m1	Parietal Endoderm	22,68	22,32	24,34	129	27
E4	*Lamc1*	Lamc1-Mm00711820_m1	Parietal Endoderm	24,87	24,81	26,08	105	37
E5	*Lefty2*	Lefty2-Mm00774547_m1	Stem Cell	nd	39,06	nd	194	nd
E6	*Lifr*	Lifr-Mm00442940_m1	Stem Cell	30,31	29,62	30,9	163	54
E7	*Lin28*	Lin28-Mm00524077_m1	Stem Cell	nd	nd	nd	nd	nd
E8	*Myf5*	Myf5-Mm00435125_m1	Muscle	nd	39,62	nd	132	nd
E9	*Myod1*	Myod1-Mm00440387_m1	Muscle	nd	nd	nd	nd	nd
E10	*Nanog*	Nanog-Mm02019550_s1	Stem Cell	35,7	34,5	38,63	232	10
E11	*Nes*	Nes-Mm00450205_m1	Neural	23,26	23,62	24,29	78	42
E12	*Neurod1*	Neurod1-Mm01946604_s1	Neural	nd	nd	nd	nd	nd
F1	*Nodal*	Nodal-Mm00443040_m1	Stem Cell	nd	nd	nd	nd	nd
F2	*Nog*	Nog-Mm00476456_s1	Stem Cell	nd	nd	nd	nd	nd
F3	*Nppa*	Nppa-Mm01255747_g1	Cardiac Muscle	nd	nd	nd	nd	nd
F4	*Nr5a2*	Nr5a2-Mm00446088_m1	Stem Cell	nd	nd	nd	nd	nd
F5	*Nr6a1*	Nr6a1-Mm00599848_m1	Stem Cell	30,44	30,2	31,06	119	53
F6	*Olig2*	Olig2-Mm01210556_m1	Oligodendrocytes	27,26	29,03	29,13	30	23
F7	*Pax4*	Pax4-Mm01159036_m1	Pancreas	38,09	37,12	36,35	198	264
F8	*Pax6*	Pax6-Mm00443072_m1	Neural	26,84	27,07	27,68	86	47
F9	*Pecam1*	Pecam1-Mm00476702_m1	Endothelial	34,4	35,18	35,56	59	36
F10	*Podxl*	Podxl-Mm00449829_m1	Stem Cell	32,16	30,78	32,95	263	47
F11	*Pou5f1*	Pou5f1-Mm00658129_gH	Stem Cell	nd	38,28	nd	333	nd
F12	*Pten*	Pten-Mm00477210_m1	Stem Cell	24,72	24,72	25,94	101	36
G1	*Ptf1a*	Ptf1a-Mm00479622_m1	Endoderm	37,61	nd	nd	19	15
G2	*Rest*	Rest-Mm00803268_m1	Stem Cell	26,91	26,94	27,7	99	48
G3	*Runx2*	Runx2-Mm00501578_m1	Bone	nd	nd	nd	nd	nd
G4	*Sema3a*	Sema3a-Mm00436469_m1	Stem Cell	32,99	30,59	33,51	533	56
G5	*Serpina1a*	Serpina1a-Mm02748447_g1	Viseral Endoderm	nd	nd	nd	nd	nd
G6	*Sfrp2*	Sfrp2-Mm00485986_m1	Stem Cell	nd	nd	nd	nd	nd
G7	*Sox17*	Sox17-Mm00488363_m1	Parietal Endoderm	nd	nd	nd	nd	nd
G8	*Sox2*	Sox2-Mm00488369_s1	Stem Cell	23,76	23,05	23,74	165	87
G9	*Sycp3*	Sycp3-Mm00488519_m1	Germ Cell	36,55	35,73	37,25	178	48
G10	*Syp*	Syp-Mm00436850_m1	Neurons	32,04	34,56	33,75	18	25
G11	*T*	T-Mm00436877_m1	Mesoderm	nd	38,78	39,54	236	107
G12	*Tat*	Tat-Mm01244282_m1	Hepatocytes	nd	nd	nd	nd	nd
H1	*Tdgf1*	Tdgf1-Mm00783944_g1	Stem Cell	39,87	37,11	38,9	685	152
H2	*Tert*	Tert-Mm00436931_m1	Stem Cell	30,25	30,86	31,46	66	35
H3	*Tcfcp2l1*	Tcfcp2l1-Mm00470119_m1	Stem Cell	32,49	33,91	32,23	38	97
H4	*Th*	Th-Mm00447546_m1	Dopamanergic Neurons	nd	36,25	38,04	1360	304
H5	*Utf1*	Utf1-Mm00447703_g1	Stem Cell	nd	nd	nd	nd	nd
H6	*Wt1*	Wt1-Mm00460570_m1	Mesoderm	nd	nd	nd	nd	nd
H7	*Xist*	Xist-Mm01232884_m1	Stem Cell	39,92	37,42	nd	572	73
H8	*Zfp42*	Zfp42-Mm01194090_g1	Stem Cell	nd	38,5	nd	286	nd
H9	*Eras*	Eras-Mm01345955_s1	Stem RAS	nd	nd	nd	nd	nd
H10	*Raf1*	Raf1-Mm00466513_m1	Radioresistance	24,02	24,17	24,72	91	52
H11	*Ctnnb1*	Ctnnb1-Mm00483033_m1	Protooncogene	22,76	23,17	24,24	76	31
H12	*Eef1a1*	Eef1a1-Mm01966109_u1	Transl. Elong. Factor	15.7	15.86	16.65	73	38